Atmos. Chem. Phys., 22, 3275–3302, 2022
https://doi.org/10.5194/acp-22-3275-2022

Atmospheric Chemistry and Physics
Open Access
EGU

Amplified role of potential HONO sources in O_3 formation in North China Plain during autumn haze aggravating processes

Jingwei Zhang[1,★], Chaofan Lian[2,3,★], Weigang Wang[2,3], Maofa Ge[2,3,7], Yitian Guo[1,4], Haiyan Ran[1,4], Yusheng Zhang[5], Feixue Zheng[5], Xiaolong Fan[5], Chao Yan[6], Kaspar R. Daellenbach[6], Yongchun Liu[5], Markku Kulmala[5,6], and Junling An[1,4,7]

[1]State Key Laboratory of Atmospheric Boundary Layer Physics and Atmospheric Chemistry (LAPC), Institute of Atmospheric Physics (IAP), Chinese Academy of Sciences, Beijing 100029, China
[2]State Key Laboratory for Structural Chemistry of Unstable and Stable Species, Beijing National Laboratory for Molecular Sciences (BNLMS), CAS Research/Education Center for Excellence in Molecular Sciences, Institute of Chemistry, Chinese Academy of Sciences, Beijing 100190, China
[3]School of Chemical Sciences, University of Chinese Academy of Sciences, Beijing 100049, China
[4]College of Earth and Planetary Sciences, University of the Chinese Academy of Sciences, Beijing 100049, China
[5]Aerosol and Haze Laboratory, Advanced Innovation Center for Soft Matter Science and Engineering, Beijing University of Chemical Technology, Beijing, 100029, China
[6]Institute for Atmospheric and Earth System Research/Physics, Faculty of Science, P.O. Box 64, 00014 University of Helsinki, Helsinki, Finland
[7]Center for Excellence in Urban Atmospheric Environment, Institute of Urban Environment, Chinese Academy of Sciences, Xiamen 361021, China
★These authors contributed equally to this work.

Correspondence: Weigang Wang (wangwg@iccas.ac.cn) and Junling An (anjl@mail.iap.ac.cn)

Received: 5 November 2021 – Discussion started: 6 December 2021
Revised: 28 January 2022 – Accepted: 4 February 2022 – Published: 11 March 2022

Abstract. Co-occurrences of high concentrations of $PM_{2.5}$ and ozone (O_3) have been frequently observed in haze-aggravating processes in the North China Plain (NCP) over the past few years. Higher O_3 concentrations on hazy days were hypothesized to be related to nitrous acid (HONO), but the key sources of HONO enhancing O_3 during haze-aggravating processes remain unclear. We added six potential HONO sources, i.e., four ground-based (traffic, soil, and indoor emissions, and the NO_2 heterogeneous reaction on ground surface (Het_{ground})) sources, and two aerosol-related (the NO_2 heterogeneous reaction on aerosol surfaces ($Het_{aerosol}$) and nitrate photolysis ($Phot_{nitrate}$)) sources into the WRF-Chem model and designed 23 simulation scenarios to explore the unclear key sources. The results indicate that ground-based HONO sources producing HONO enhancements showed a rapid decrease with height, while the NO + OH reaction and aerosol-related HONO sources decreased slowly with height. $Phot_{nitrate}$ contributions to HONO concentrations were enhanced with aggravated pollution levels. The enhancement of HONO due to $Phot_{nitrate}$ on hazy days was about 10 times greater than on clean days and $Phot_{nitrate}$ dominated daytime HONO sources ($\sim$ 30 %–70 % when the ratio of the photolysis frequency of nitrate ($J_{nitrate}$) to gas nitric acid (J_{HNO_3}) equals 30) at higher layers (>800 m). Compared with that on clean days, the $Phot_{nitrate}$ contribution to the enhanced daily maximum 8 h averaged (DMA8) O_3 was increased by over 1 magnitude during the haze-aggravating process. $Phot_{nitrate}$ contributed only $\sim$ 5 % of the surface HONO in the daytime with a $J_{nitrate}/J_{HNO_3}$ ratio of 30 but contributed $\sim$ 30 %–50 % of the enhanced O_3 near the surface in NCP on hazy days. Surface O_3 was dominated by volatile organic compound-sensitive chemistry, while O_3 at

higher altitudes (>800 m) was dominated by NO_x-sensitive chemistry. $Phot_{nitrate}$ had a limited impact on nitrate concentrations (<15 %) even with a $J_{nitrate}/J_{HNO_3}$ ratio of 120. These results suggest the potential but significant impact of $Phot_{nitrate}$ on O_3 formation, and that more comprehensive studies on $Phot_{nitrate}$ in the atmosphere are still needed.

1 Introduction

Nitrous acid (HONO) is an important source of the hydroxyl radical (OH) through its photolysis (Reaction R1), and contributes ∼ 20 %–80 % of primary OH production (Alicke et al., 2002; Hendrick et al., 2014; Kim et al., 2014).

$$HONO + h\nu \rightarrow NO + OH. \quad (R1)$$

Although 40 years have passed since the first detection of HONO in the atmosphere (Perner and Platt, 1979), the sources of HONO (especially daytime) and the dynamic parameters of HONO formation mechanisms are still not well understood (Ge et al., 2021). Current air quality models with the default gas-phase reaction (the reverse reaction of Reaction R1) always significantly underestimate HONO observations, resulting in low atmospheric oxidation capacity and in underestimation of secondary pollutants such as ozone (O_3) (Li et al., 2010, 2011; Sarwar et al., 2008; Zhang et al., 2016, 2019a).

HONO sources can be generally classified into three categories, i.e., direct emissions and homogeneous and heterogeneous reactions. Direction emissions are mainly from traffic (Kramer et al., 2020; Kurtenbach et al., 2001; Liao et al., 2021), soil (Kubota and Asami, 1985; Oswald et al., 2013; Wu et al., 2019; Xue et al., 2021), biomass burning (Cui et al., 2021; Rondon and Sanhueza, 1989; Theys et al., 2020), and indoor combustion processes (Klosterkother et al., 2021; Liu et al., 2019; Pitts et al., 1985). The reaction of nitric oxide (NO) with OH (Pagsberg et al., 1997; Stuhl and Niki, 1972) is usually thought to be the dominant homogeneous reaction and is significant during daytime, but may be neglected at night due to low OH concentrations, other minor homogeneous HONO sources including nucleation of NO_2, H_2O, and NH_3 (Zhang and Tao, 2010), via the photolysis of orthonitrophenols (Bejan et al., 2006; Chen et al., 2021; Lee et al., 2016), via the electronically excited NO_2 and H_2O (Crowley and Carl, 1997; Dillon and Crowley, 2018; Li et al., 2008) and via $HO_2{\cdot}H_2O + NO_2$ reaction (Li et al., 2015, 2014; Ye et al., 2015). The heterogeneous reactions mainly include nitrogen dioxide (NO_2) hydrolysis and reduction reactions on various humid surfaces (Finlayson-Pitts et al., 2003; Ge et al., 2019; Gómez Alvarez et al., 2014; Ma et al., 2013; Marion et al., 2021; Sakamaki et al., 1983; Tang et al., 2017; W. Yang et al., 2021) and nitrate photolysis ($Phot_{nitrate}$) (Romer et al., 2018; Ye et al., 2016a, b; Zhou et al., 2003), and are usually considered the main contributors to HONO concentrations in the atmosphere.

Among these potential HONO sources, the photolysis of nitrate to produce HONO in the atmosphere has received extensive attention over the past few years, and the $Phot_{nitrate}$ frequency ($J_{nitrate}$) is still debated (Gen et al.., 2022). In laboratory studies, some researchers (Bao et al., 2018; Ye et al., 2016a, 2017) showed that $Phot_{nitrate}$ was an important HONO source, the measured $J_{nitrate}$ was 1–3 orders larger than the gas nitric acid (HNO_3) photolysis frequency (J_{HNO_3}) and could reach up to $10^{-4}\ s^{-1}$. Furthermore, a number of substances including humic acid (Yang et al., 2018), sulfate (Bao et al., 2020), and TiO_2 (Xu et al., 2021) might enhance the reaction significantly; while Shi et al. (2021) found that the $J_{nitrate}/J_{HNO_3}$ ratio was <10 when using suspended submicron particulate sodium and ammonium nitrate rather than $PM_{2.5}$ samples. In field studies combined with model simulations, Kasibhatla et al. (2018) compared NO_x observations from the Cape Verde Atmospheric Observatory with GEOS-Chem (Goddard Earth Observing System-Chemistry) model simulations and reported a $J_{nitrate}/J_{HNO_3}$ ratio of 25–50; Romer et al. (2018) reported a $J_{nitrate}/J_{HNO_3}$ ratio of <30 based on observations of NO_x (= NO + NO_2) and HNO_3 over the Yellow Sea and a box model simulation, while larger $J_{nitrate}/J_{HNO_3}$ ratios (e.g., 300) were inconsistent with the observed NO_x to HNO_3 ratios. Adopting a $J_{nitrate}/J_{HNO_3}$ ratio of ∼ 120 could greatly improve daytime surface HONO simulations (contributed ∼ 30 %–40 % of noontime HONO) by using the Community Multiscale Air Quality model (CMAQ) in the Pearl River Delta (Fu et al., 2019) or a box model in the Yangtze River Delta (Shi et al., 2020), whereas a $J_{nitrate}/J_{HNO_3}$ ratio of 30 produced negligible HONO in clean periods (∼ 2 %) and slightly higher HONO in heavy haze periods (∼ 8 %) in the North China Plain (NCP) by using a box model (Xue et al., 2020) and ∼ 1 % by using CMAQ in urban Beijing (Zhang et al., 2021). Recently, Zheng et al. (2020) evaluated the effect of three $J_{nitrate}/J_{HNO_3}$ ratios (1, 10, and 100) on heterogeneous sulfate formation by using CMAQ and large uncertainties of simulated sulfate concentrations were reported. The most widely adopted $J_{nitrate}/J_{HNO_3}$ ratios were 1–30 or 100–120 with large uncertainties, and thus more efforts are needed to better understand the $Phot_{nitrate}$ impact on atmospheric oxidation capacity and on concentrations of HONO and other secondary pollutants.

A number of potential HONO sources (e.g., direct emissions, NO_2 heterogeneous reactions, and $Phot_{nitrate}$) have been coupled into several air quality models (An et al., 2013; Fu et al., 2019; Guo et al., 2020; Li et al., 2010, 2011; Sar-

war et al., 2008; Tang et al., 2015; Xu et al., 2006; Zhang et al., 2019a, b, 2021, 2022; J. Zhang et al. 2020) to improve HONO simulations. The improved HONO sources can produce more OH, which is favorable for the formation of O_3 (Fu et al., 2019; Guo et al., 2020; Li et al., 2010; Xing et al., 2019; Zhang et al., 2016, 2019a, 2022). O_3 can directly damage plants and threaten human health (Avnery et al., 2011a, b; Feng et al., 2015, 2019, 2022; Mills et al., 2007, 2018; Richards et al., 1958; Selin et al., 2009; Wilkinson et al., 2012; Zhao et al., 2021), and an increasing trend of O_3 concentrations in China has been widely reported in recent years (S. Chen et al., 2020; Li et al., 2020; Lu et al., 2020; Ma et al., 2016; Maji and Namdeo, 2021), making O_3 pollution a severe concern. A co-occurrence of high $PM_{2.5}$ and O_3 concentrations has been frequently reported in China over the past few years, with researchers speculating a significant role of HONO in producing O_3 enhancements (Feng et al., 2021; Fu et al., 2019; Tie et al., 2019; K. Yang et al., 2021). Nevertheless, current knowledge on the HONO difference in O_3 formation during clean and hazy days is still unclear, especially the relative contribution of each potential HONO source to O_3 enhancements during haze-aggravating processes with a co-occurrence of high $PM_{2.5}$ and O_3 concentrations.

In this study, time series of pollutants including HONO, O_3, and nitrate were collected in NCP during 11–31 October 2018, in which high concentrations of $PM_{2.5}$ accompanied by high O_3 concentrations were found at least twice during haze events. The specific role of each potential HONO source in O_3 formation is explored during these haze events by coupling the potential HONO sources into the Weather Research and Forecasting model with Chemistry (WRF-Chem, Grell et al., 2005). The relative contribution of each potential HONO source to surface-averaged and vertically averaged concentrations of HONO and O_3 are quantified and the uncertainty in key potential HONO sources (e.g., J_{nitrate}) is discussed, in order to find the key HONO sources resulting in O_3 enhancements in NCP at different pollution levels (especially during haze-aggravating processes).

2 Data and methods

2.1 Observation data

The field observation was carried out during 11–31 October 2018, and the observation site was located on the west campus of Beijing University of Chemical Technology (BUCT, 116°18′37″ E, 39°56′56″ N) in Beijing. BUCT is an urban site close to the third ring road of Beijing, with extensive human activities, including vehicle emissions. Instruments were set up on the fifth floor of the main teaching building. HONO was measured with a home-made water-based long-path absorption photometer (Y. Chen et al., 2020). A dual-channel absorption system was deployed to subtract the potential interferences, e.g., NO_2 hydrolysis. A set of on-line commercial analyzers (Thermo 48i, 42i, 49i, 43i) was used for measurements of CO, NO_x, O_3, and SO_2. Specifically, the 42i used a molybdenum NO_2-to-NO converter, and there would be an NO_2 overestimation for the conversion of HONO, HNO_3, or other NO_y. Considering the relatively lower concentration compared with NO_2, the impact would be minor. The chemical composition of $PM_{2.5}$ was analyzed with a Time-of-Flight Aerosol Chemical Speciation Monitor (ToF-ACSM, Aerodyne). ToF-ACSM was developed by Fröhlich et al. (2013) for non-refractory $PM_{2.5}$ measurement. Details on its usage can be found in Liu et al. (2020), where ionization efficiency calibration of nitrate was performed using 300 nm dry NH_4NO_3 every month during the observation period. An online single-photon ionization time-of-flight mass spectrometer (SPI-ToF-MS, Hexin) was used for the detection of a large variety of volatile organic compounds (VOCs) (Gao et al., 2013). Surface observations of O_3, NO_2, $PM_{2.5}$, and PM_{10} at 95 sites in NCP were obtained from https://quotsoft.net/air/ (last access: 3 March 2022), issued by the China Ministry of Ecology and Environment; surface meteorological observations at 284 sites in NCP were taken from the National Climatic Data Center, China Meteorological Administration (Fig. 1).

Vertical HONO observations were not available during the period 11–31 October 2018 at the BUCT site, and we therefore used the observed vertical HONO concentrations from Meng et al. (2020) in urban Beijing in December 2016 to evaluate our simulation of vertical HONO concentrations, which were also used by Zhang et al. (2021) in their CMAQ evaluation.

2.2 Model description

The improved WRF-Chem model (version 3.7.1), which included six potential HONO sources, i.e., traffic (E_{traffic}), soil (E_{soil}), and indoor (E_{indoor}) emissions, $\mathrm{Phot}_{\mathrm{nitrate}}$ in the atmosphere, and NO_2 heterogeneous reactions on aerosol ($\mathrm{Het}_{\mathrm{aerosol}}$) and ground ($\mathrm{Het}_{\mathrm{ground}}$) surfaces (Zhang et al., 2019a), was used in this study. $\mathrm{Phot}_{\mathrm{nitrate}}$ was newly added in WRF-Chem (Reaction R2) following the work of Fu et al. (2019), Ye et al. (2017), and Zhou et al. (2003):

$$p\mathrm{NO_3} + h\nu \rightarrow 0.67\mathrm{HONO} + 0.33\mathrm{NO_2}. \quad \text{(R2)}$$

For $\mathrm{Het}_{\mathrm{aerosol}}$ and $\mathrm{Het}_{\mathrm{ground}}$, laboratory studies suggest that these heterogeneous reactions of NO_2 to HONO are of first order in NO_2 (Aumont et al., 2003; Finlayson-Pitts et al., 2003; Saliba et al., 2000):

$$\mathrm{NO_2} \rightarrow \mathrm{HONO}\ \ k_{\mathrm{a}}, \quad \text{(R3)}$$

$$\mathrm{NO_2} \rightarrow \mathrm{HONO}\ \ k_{\mathrm{g}}. \quad \text{(R4)}$$

The first-order rate constants for aerosol (k_{a}) and ground (k_{g}) surface reactions are calculated as:

$$k_{\mathrm{a}} = \frac{1}{4} \times v_{\mathrm{NO_2}} \times \left(\frac{S}{V}\right) \times \gamma, \quad (1)$$

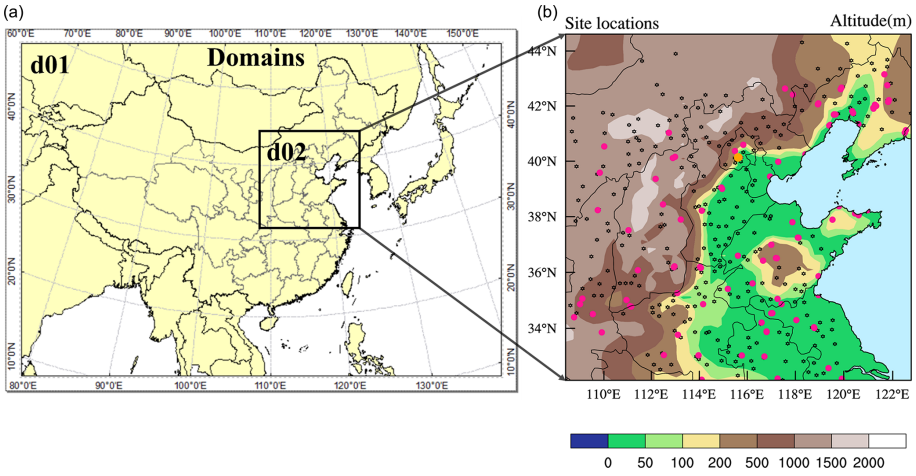

Figure 1. Domains of WRF-Chem used in this study **(a)**, and the locations of one HONO observation site (orange dot in urban Beijing), 95 environmental monitoring ($PM_{2.5}$, NO_2 and O_3) sites (dark pink dots), and 284 meteorological observation sites (black dots) in domain 2 **(b)**.

$$k_g = \frac{f \times v_d}{H}, \tag{2}$$

where v_{NO_2} is the mean molecular speed of NO_2, $\frac{S}{V}$ is the surface-to-volume ratio for aerosols, γ is the reactive uptake coefficient of aerosols, f is the proportion of deposited NO_2 reaching the surface in participating HONO formation, v_d is the dry deposition velocity of NO_2, and H is the first model layer height above the ground (~ 35 m). It should be noted that not 100 % (50 % is commonly accepted) of the participating NO_2 could be converted to HONO in Reactions (R3) and (R4), and thus k_a and k_g were multiplied by 0.5 in the final calculation of HONO heterogeneous formation via NO_2.

The two factors γ and f were improved from previous studies (Li et al., 2010; Liu et al., 2014; Zhang et al., 2019a) and calculated by:

$$\gamma = 5 \times 10^{-6} \times \left(1 + \frac{SR}{\alpha}\right), \tag{3}$$

$$f = 0.08 \times \left(1 + \frac{SR}{\alpha}\right), \tag{4}$$

where SR denotes solar radiation (W m^{-2}), α is an adjusted parameter and set as 100 (W m^{-2}), and thus γ and f become continuous functions during the whole day (γ and f enhanced by 10 times and reached 5×10^{-5} and 0.8 when SR reached 900 W m^{-2} at noontime, respectively).

The physical and chemical schemes used in this study are given in Table 1. Two domains were adopted, domain one contains 82×64 grid cells with a horizontal resolution of 81 km, and domain two contains 51×51 grid cells with a horizontal resolution of 27 km (Fig. 1), both with 17 vertical layers encompassing from the surface to 100 hPa. The observational sites are shown in the right panel of Fig. 1, including one HONO observation site (the orange dot in urban Beijing), 95 observation sites of $PM_{2.5}$, NO_2, and O_3 (pink dots), and 284 meteorological monitoring sites (black dots).

The anthropogenic emissions in East Asia in 2010 were taken from the MIX emission inventory (Li et al., 2017) (http://www.meicmodel.org/, last access: 3 March 2022), including both gaseous and aerosol species, i.e., SO_2, NO_x, CO, VOCs, NH_3, PM_{10}, $PM_{2.5}$, BC, OC, and CO_2, and were provided monthly by five sectors (power, industry, residential, transportation, and agriculture) at a resolution of $0.25° \times 0.25°$. VOC emissions were speciated into model-ready inputs according to the MOZART chemical mechanism to build the WRF-Chem emission files. The anthropogenic emissions in China were replaced by employing the MEIC 2016 (the Multi-resolution Emission Inventory for China) developed by Tsinghua University. The NH_3 emissions in China were from Dong et al. (2010), biomass burning emissions were from Huang et al. (2012), and biogenic emissions were calculated using the Model of Emissions of Gases and Aerosols from Nature (MEGAN) (Guenther et al., 2012). Due to the sharp reduction in anthropogenic emissions in recent years, the default emission inventory was systematically overestimated in autumn of 2018, especially for SO_2 and $PM_{2.5}$ concentrations. Based on the comparison of simulations and observations (the urban Beijing site plus the other 95 pollutant-monitoring sites in NCP), we cut off 80 % of SO_2 emissions, 50 % of NH_3 emissions, 30 % of toluene emissions, and 50 % of $PM_{2.5}$ and PM_{10} emissions. The cut-off emissions are largely close to the emission reductions in east China during the period 2013–2017 (Zhang and Geng, 2019). The revised emissions significantly improved regional $PM_{2.5}$ simulations in NCP (Fig. S1), and the simulations of gases and $PM_{2.5}$ in urban Beijing (Fig. S2).

The National Centers for Environmental Prediction (NCEP) $1° \times 1°$ final reanalysis data (FNL) (https://rda.ucar.

Table 1. Physical and chemical options in WRF-Chem used in this study.

Options	WRF-Chem
Advection scheme	Runge–Kutta 3rd order
Boundary layer scheme	YSU
Cloud microphysics	Lin et al. (1983)
Cumulus parameterization	New Grell scheme
Land-surface model	Noah
Long-wave radiation	RRTM
Short-wave radiation	Goddard
Surface layer	Revised MM5 Monin–Obukhov scheme
Aerosol option	MOSAIC (Zaveri et al., 2008)
Chemistry option	Updated MOZART mechanism (Emmons et al., 2010)
Photolysis scheme	F-TUV

edu/datasets/ds083.2/, last access: 3 March 2022, National Centers for Environmental Prediction et al., 2000) were used in this study to obtain the meteorological initial and boundary conditions every 6 h. The global simulations of MOZART-4 (https://www.acom.ucar.edu/wrf-chem/mozart.shtml, last access: 3 March 2022) were used as the chemical initial and boundary conditions (every 6 h).

In total, 23 simulation scenarios were performed in this study (Table 2), in which the base case only considered the default homogeneous reaction ($OH + NO \rightarrow HONO$), case 6S contained six potential HONO sources while cases A, B, C, D, E, and F contained each of the six potential HONO sources, respectively. The other 15 cases (A_double, A_half, ... , Nit_120, D_NO_2, and D_HONO) were used to evaluate the uncertainties of the six potential HONO sources (Table 2). All of the cases were simulated with a spin-up of 7 d. $J_{nitrate}$ and J_{HNO_3} denote the photolysis frequency of nitrate and gas nitric acid in the atmosphere, respectively. The enhancement factor for F_double was 1.25 instead of 2.0 to avoid the production rate of HONO from NO_2 reaching the surface exceeding 100 %. The 0.33NO_2 in D_NO_2 or 0.67HONO in D_HONO referred to the assumed $Phot_{nitrate}$ products in Reaction (R2).

3 Results

3.1 Comparison of simulations and observations

3.1.1 Meteorological factors

The statistical metrics of simulated meteorological parameters at 284 sites in NCP including air temperature (T), relative humidity (RH), and wind speed (WS) were comparable with the modeling results reported by other researchers (Table 3). The simulated wind direction (WD) bias within 45° accounted for ∼ 56 %, and the bias within 90° accounted for ∼ 80 %, suggesting that the simulated WD captured the main observed WD.

3.1.2 Pollutant concentrations at the BUCT site

Time series of the observational data at the BUCT site are shown in Fig. 2, the gray-shaded periods stand for three haze-aggravating processes, while the cyan-shaded period denotes typical clean days. The largest hourly observations of O_3 (∼ 50–75 ppb) and $PM_{2.5}$ (∼ 100–200 µg m^{-3}) were both relatively higher on hazy days than on clean days, especially for the first two haze events (the O_3 concentrations in the third haze event were relatively lower due to the higher NO_x concentrations in the urban area).

The observed $PM_{2.5}$ and nitrate trends at the BUCT site were well simulated (Fig. 2a and b), and NO_2 simulations generally agreed with the observations (Fig. 2c). The promotion effect of the six potential HONO sources on the formation of secondary aerosols leads to an increase in concentrations of $PM_{2.5}$ and nitrate for case 6S, despite nitrate consumption through $Phot_{nitrate}$ (Li et al., 2010; Qu et al., 2019; Fu et al., 2019; Zhang et al., 2019a, 2021); detailed nitrate variation caused by each of the six potential HONO sources in case 6S is presented in Fig. S3. The overestimation of nitrate could be partially caused by the uncertainties in the anthropogenic emission inventory, e.g., the overestimation of NO_x emissions (Fig. 2c). The inadequate understanding of the nitrate formation mechanism could also be related to nitrate simulation bias, which was also found in some related studies using CMAQ (Fu et al., 2019; Zhang et al., 2021).

Hourly and diurnal HONO simulations at the BUCT site (Figs. 2d and 3a) were significantly improved in the 6S case (mean of 1.47 ppb) compared with the base case (mean of 0.05 ppb). The normalized mean bias (NMB) was remarkably reduced to −14.22 % (6S) from −97.11 % (Base), and the index of agreement (IOA) was improved significantly to 0.80 (6S) from 0.45 (Base) (Fig. 2d). The underestimation of the simulated HONO (6S) on 15 and 22 October was mainly caused by the earlier scavenging of pollutants at the BUCT site in the model used (Fig. 2a and d).

As for O_3, noticeable improvements were found at the BUCT site after considering the six potential HONO sources,

Table 2. Simulation scenarios designed in this study.

Case	HONO sources
Base	Default (OH + NO → HONO)
6S	Default + $E_{traffic}$ + E_{soil} + E_{indoor} + $Phot_{nitrate}$ ($J_{nitrate}/J_{HNO_3} = 30$) + $Het_{aerosol}$ + Het_{ground}
A	Default + $E_{traffic}$
B	Default + E_{soil}
C	Default + E_{indoor}
D	Default + $Phot_{nitrate}$ ($J_{nitrate}/J_{HNO_3} = 30$)
E	Default + $Het_{aerosol}$
F	Default + Het_{ground}
A_double	Default + $2 \times E_{traffic}$
A_half	Default + $0.5 \times E_{traffic}$
B_double	Default + $2 \times E_{soil}$
B_half	Default + $0.5 \times E_{soil}$
C_double	Default + $2 \times E_{indoor}$
C_half	Default + $0.5 \times E_{indoor}$
E_double	Default + $Het_{aerosol}$ ($2 \times \gamma$)
E_half	Default + $Het_{aerosol}$ ($0.5 \times \gamma$)
F_double	Default + Het_{ground} ($1.25 \times f$)
F_half	Default + Het_{ground} ($0.5 \times f$)
Nit_1	Default + $Phot_{nitrate}$ ($J_{nitrate}/J_{HNO_3} = 1$)
Nit_7	Default + $Phot_{nitrate}$ ($J_{nitrate}/J_{HNO_3} = 7$)
Nit_120	Default + $Phot_{nitrate}$ ($J_{nitrate}/J_{HNO_3} = 120$)
D_NO_2	Only 0.33NO_2 produced in $Phot_{nitrate}$ for case D
D_HONO	Only 0.67HONO produced in $Phot_{nitrate}$ for case D

Table 3. Performance metrics (index of agreement (IOA), RMSE, and MB (mean bias)) of WRF-Chem simulated air temperature, relative humidity, wind speed, and direction at 284 meteorological sites in the North China Plain during 11–31 October 2018. The definitions of the metrics used in this study are given in Sect. S1.

	IOA	RMSE	MB	Reference
T (°C)	0.97	1.4	−1.1	This work
	0.90	2.5	0.2	Wang et al. (2014)
	0.90	–	−0.9	Wang et al. (2010)
	0.88	–	0.5	Li et al. (2012)
	–	3.1	0.8	Zhang et al. (2012)
RH (%)	0.90	9.0	−7.1	This work
	0.78	16.3	−5.5	Wang et al. (2014)
	0.78	–	−1.3	Wang et al. (2010)
	0.86	–	−1.1	Li et al. (2012)
	–	17.4	−5.7	Zhang et al. (2012)
WS ($m\,s^{-1}$)	0.48	1.4	1.3	This work
	0.56	2.5	1.6	Wang et al. (2014)
	0.65	2.1	0.9	Wang et al. (2010)
	0.62	1.5	0.6	Li et al. (2012)
	–	2.2	1.1	Zhang et al. (2012)
WD Bias	0–45°	45–90°	>90°	
Count	75 701	21 500	28 075	135 276 (Total)
Percentage	55.96 %	23.29 %	20.75 %	

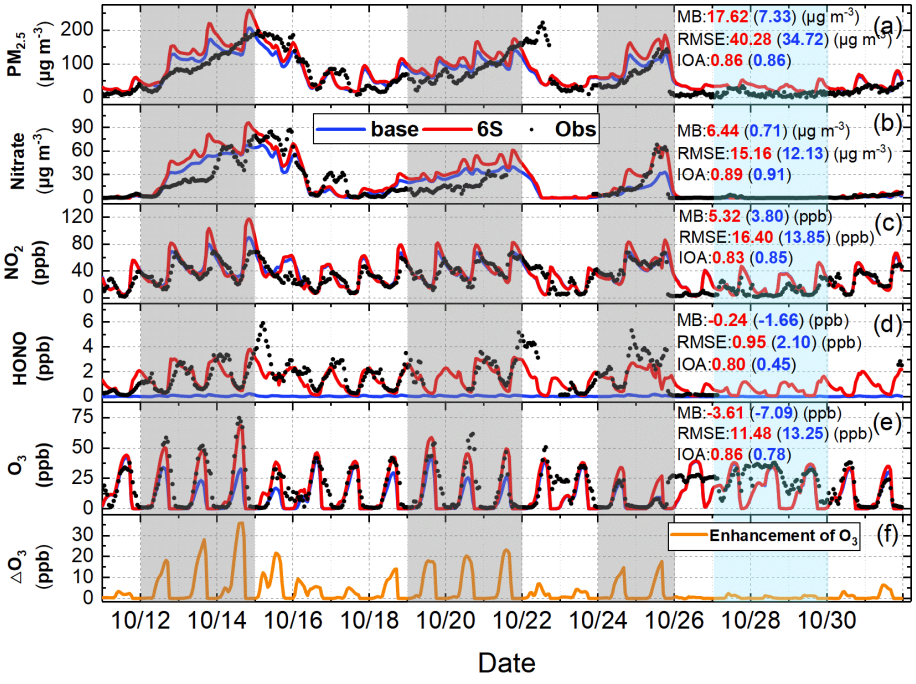

Figure 2. Comparison of simulated (Base and 6S cases) and observed hourly concentrations of $PM_{2.5}$, nitrate, NO_2, HONO, and O_3 **(a–e)**, and the hourly enhanced concentrations of O_3 (ΔO_3) **(f)** caused by the six potential HONO sources (6S minus Base) at the BUCT site during 11–31 October 2018.

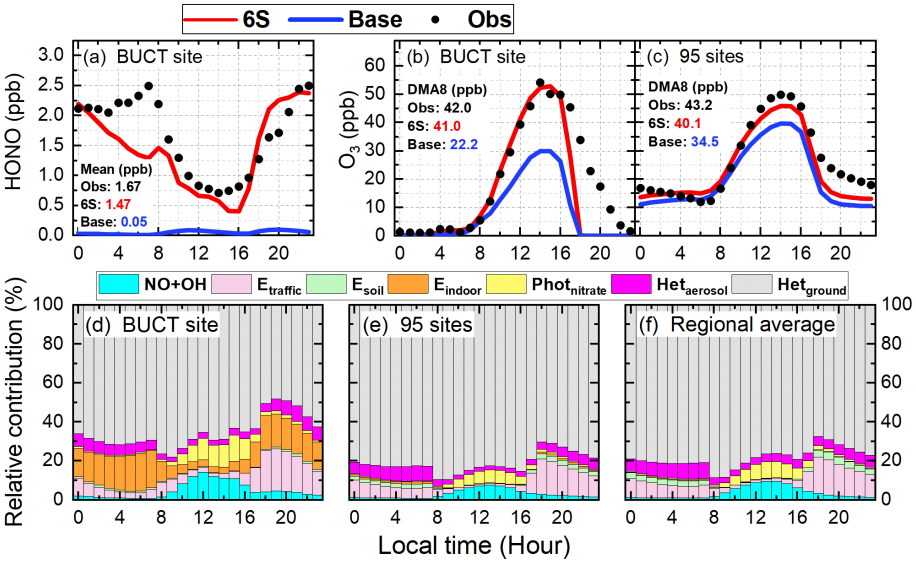

Figure 3. Comparison of diurnal mean simulations (Base and 6S cases) and observations of HONO during the study period **(a)** and O_3 during the first two haze events at the BUCT site **(b)** and O_3 averages at the 95 NCP monitoring sites during the study period **(c)**; the relative contributions of each of the six potential HONO sources and the reaction of OH with NO to surface HONO concentrations for the 6S case at the BUCT site **(d)**, at the 95 monitoring sites **(e)**, and in the whole NCP region **(f)**. The calculated 24 h mean HONO concentrations and DMA8 O_3 concentrations are given in panels **a**–**c**.

especially on hazy days (Fig. 2e and f). The mean bias (MB) was improved to −3.61 ppb (6S) from −7.09 ppb (Base), and the IOA was improved to 0.86 (6S) from 0.78 (Base) (Fig. 2e). In particular, the 6S case significantly enhanced daytime hourly O_3 by 15–35 ppb compared with the base case, and the simulated O_3 was very close to the observations on hazy days (Fig. 2e). Larger daytime O_3 enhancements were accompanied by higher $PM_{2.5}$ concentrations during haze-aggravating processes, while on clean days the daytime-enhanced O_3 due to the potential HONO sources was mostly <5 ppb (Fig. 2e and f). The diurnal O_3 pattern during the first two haze-aggravating processes is presented in Fig. 3b. Significant improvements in daily maximum 8 h (10:00–17:59) averaged (DMA8) O_3 (18.8 ppb) occurred at the BUCT site after considering the six potential HONO sources, and the NMB of DMA8 O_3 was remarkably improved to −2.38 % (6S) from −47.14 % (Base).

The relative contribution of each HONO source near the surface at the BUCT site for the 6S case is shown in Fig. 3d. Briefly, Het_{ground} was the largest source during daytime and nighttime (∼ 50 %–70 %), consistent with the results of Zhang et al. (2021). $Phot_{nitrate}$ ($J_{nitrate}/J_{HNO_3} = 30$) and the NO + OH reaction contributed similarly ∼ 1 %–12 % during daytime. The contribution of $E_{traffic}$ was significant during nighttime (∼ 10 %–20 %) but small during daytime (<5 %). The contribution of $Het_{aerosol}$ to HONO concentrations was minor (∼ 2 %–3 %) during daytime and ∼ 6 %–10 % at nighttime. E_{soil} could be neglected while the contribution of E_{indoor} was close to that of $E_{traffic}$ in urban Beijing. The relative contribution of the potential HONO sources in this study was comparable to the results reported by Fu et al. (2019) when using CMAQ, except for the contribution of $Phot_{nitrate}$ due to the different $J_{nitrate}/J_{HNO_3}$ ratios (30 in our study and ∼ 120 in Fu et al., 2019).

3.1.3 Pollutant concentrations in NCP

The 95-site-averaged hourly simulations and observations of O_3, NO_2, and $PM_{2.5}$ during the study period are shown in Fig. 4. The six potential HONO sources significantly improved hourly O_3 simulations, remarkably enhanced the daily maximum O_3 by ∼ 5–10 ppb during 11–25 October, and by ∼ 2–4 ppb during 26–31 October (Fig. 4a and b). The simulations of NO_2 agreed well with the observations, and the mean concentrations were 22.55 (Base), 21.62 (6S), and 20.74 (Obs) ppb (Fig. 4c). The $PM_{2.5}$ simulations generally followed the observed $PM_{2.5}$ trend but were overestimated by ∼ 8 μg m^{-3}, with averaged concentrations of 49.94 (Base), 53.30 (6S), and 45.31 (Obs) μg m^{-3} (Fig. 4d), respectively.

The 95-site-averaged diurnal simulations and observations of O_3 are presented in Fig. 3c. O_3 simulations showed a remarkable improvement when the six potential HONO sources were considered. The six potential HONO sources produced a mean enhancement of 5.7 ppb in DMA8 O_3 and improved the NMB to −7.16 % from −20.32 % at the 95 sites in NCP. The 95-site-averaged diurnal simulations and observations of NO_2 and $PM_{2.5}$ during the study period are demonstrated in Fig. S4. NO_2 simulations generally followed the observed trend but were underestimated from 04:00 to 16:00 and overestimated after 18:00 (Fig. S4a), $PM_{2.5}$ simulations agreed with the observed diurnal pattern but were overestimated for both cases during the whole day (Fig. S4b).

The relative contribution of each HONO source near the surface at the 95 NCP sites for the 6S case is shown in Fig. 3e. Het_{ground} was the dominant source during daytime and nighttime (∼ 70 %–80 %). $Phot_{nitrate}$ ($J_{nitrate}/J_{HNO_3} = 30$) and the NO + OH reaction nearly equaled and contributed ∼ 2 %–8 % during daytime (∼ 5 % on average). The contribution of $E_{traffic}$ was significant during nighttime (∼ 10 %–15 %) but small during daytime (<3 %). The contribution of $Het_{aerosol}$ to HONO concentrations was <3 % during daytime and <10 % at nighttime. E_{soil} contributed ∼ 3 % at nighttime but could be neglected at daytime. The contribution of E_{indoor} was too small to be noticed at the 95 NCP sites, implying that this source was noticeable only in megacities. The relative contribution of each HONO source in the whole NCP region (all grid cells in domain two except for the seas) is presented in Fig. 3f. The results were quite similar to those of the 95 sites (Fig. 3e), which were representative for the whole NCP region. To further understand the role of potential HONO sources in haze-aggravating processes in regional O_3 concentrations, the 95-site-averaged surface/vertical HONO concentrations and their impacts during a typical haze event (19–21 October) and a clean period (27–29 October) were analyzed and are presented in the following sections.

3.2 Spatial distribution of enhanced DMA8 O_3 by potential HONO sources

3.2.1 General patterns of enhanced DMA8 O_3

Figure S5 shows surface-averaged and zonal-averaged DMA8 O_3 enhancements due to the six potential HONO sources in NCP during the study period (11–31 October) and three haze events (12–14, 18–21, and 24–25 October). The overall surface DMA8 O_3 enhancement decreased gradually from south (6–10 ppb) to north (2–6 ppb) (Fig. S5a) and could reach 10–20 ppb under unfavorable meteorological conditions during haze events (Fig. S5b–d). For the first two haze events, the anti-cyclone in the Shandong peninsula carried pollutants being transported from the southeastern NCP to the western (108–112° E) and northern (39–41° N) NCP, and the six potential HONO sources led to a DMA8 O_3 enhancement of 10–20 (Fig. S5b) and 10–15 ppb (Fig. S5c) in Beijing, respectively. For the third haze event, two air masses converged to form a transport channel from south to north. The O_3 enhancement caused by the six potential HONO sources reached 10–18 ppb in the southern NCP and decreased to 6–10 ppb in the northern NCP along the transport channel. Vertically, the DMA8 O_3 enhancements were

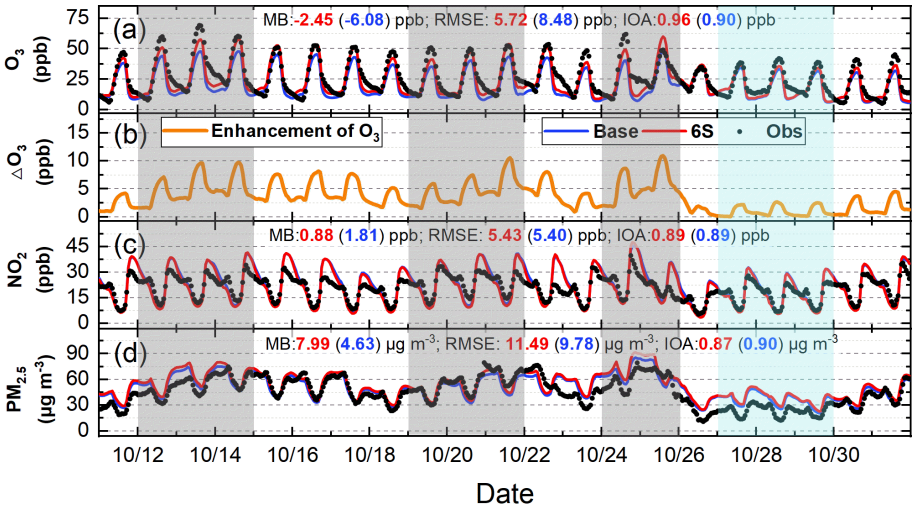

Figure 4. Comparison of 95-site-averaged hourly simulations (Base and 6S cases) and observations of O_3 **(a)**, NO_2 **(c)**, $PM_{2.5}$ **(d)**, and O_3 enhancements due to the six potential HONO sources (6S minus Base case) **(b)** in the North China Plain during 11–31 October 2018.

2–8 ppb during the whole period (Fig. S5e) and increased to 6–12 ppb in these haze events (Fig. S5f–h). The enhanced O_3 near the surface (0–100 m) was slightly smaller than that at higher altitude (Fig. S5f–h), due mainly to the stronger titration of O_3 by NO near the surface. These results demonstrate that the six potential HONO sources significantly enhanced surface and vertical O_3 concentrations in NCP, especially during haze events.

3.2.2 Enhanced DMA8 O_3 during a typical haze-aggravating process and a clean period

Figure 5 demonstrates surface-averaged and zonally averaged DMA8 O_3 enhancements due to the six potential HONO sources in NCP during a typical haze-aggravating process (19–21 October 2018) and a clean period (27–29 October 2018). The increasing trend of DMA8 O_3 enhancements can be clearly seen from 19 to 21 October near the surface and in the vertical direction. During the haze-aggravating process, the surface DMA8 O_3 enhancements were ∼2–10 ppb (19 October), ∼6–12 ppb (20 October), and ∼8–15 ppb (21 October), respectively; the vertical DMA8 O_3 enhancements were ∼4–7 ppb (19 October), ∼6–10 ppb (20 October), and ∼8–15 ppb (21 October), respectively. While during clean days, the surface/vertical DMA8 O_3 enhancements were usually <4 ppb. The six potential HONO sources significantly enhanced surface and vertical O_3 concentrations in NCP during haze-aggravating processes. The detailed role of the potential HONO sources in vertical HONO concentrations and their impacts are presented in the next section.

3.3 Vertical variations of the six potential HONO sources and their impacts

3.3.1 Six potential HONO sources and their impacts on HONO concentrations

A number of studies have conducted vertical HONO observations abroad (Kleffmann et al., 2003; Ryan et al., 2018; Sörgel et al., 2011; VandenBoer et al., 2013; Villena et al., 2011; Wang et al., 2020; Wong et al., 2011, 2012; Zhang et al., 2009) and in China (Meng et al., 2020; Wang et al., 2019; Xing et al., 2021; Zhu et al., 2011). A decreasing trend of HONO with height was mostly observed in these studies, and our simulations also reproduced this vertical variation and were comparable to another model simulation by Zhang et al. (2021), who used CMAQ (Fig. S6). For an in-depth understanding of the role of each HONO source considered in HONO concentrations at different heights, we assessed the contributions of each potential HONO source to HONO concentrations at different heights (Fig. 6) during 11–31 October 2018.

Generally, the impacts of ground-based potential HONO sources ($E_{traffic}$, E_{soil}, E_{indoor}, and Het_{ground}) on HONO concentrations decreased rapidly with height, while the NO + OH reaction and aerosol-related HONO sources ($Phot_{nitrate}$ and $Het_{aerosol}$) decreased slowly with height (Fig. 6). During daytime the NO + OH reaction, $Phot_{nitrate}$, and Het_{ground} were the three main HONO sources, while during nighttime $E_{traffic}$, $Het_{aerosol}$, and Het_{ground} were the three main contributors to HONO concentrations (Fig. 6). The HONO concentrations via the NO + OH reaction and $Phot_{nitrate}$ were higher during daytime. The impact of E_{soil} in the NCP was small; nevertheless, Xue et al. (2021) found strong soil HONO emissions in NCP agricultural fields after fertilization, suggesting that this source may have a signifi-

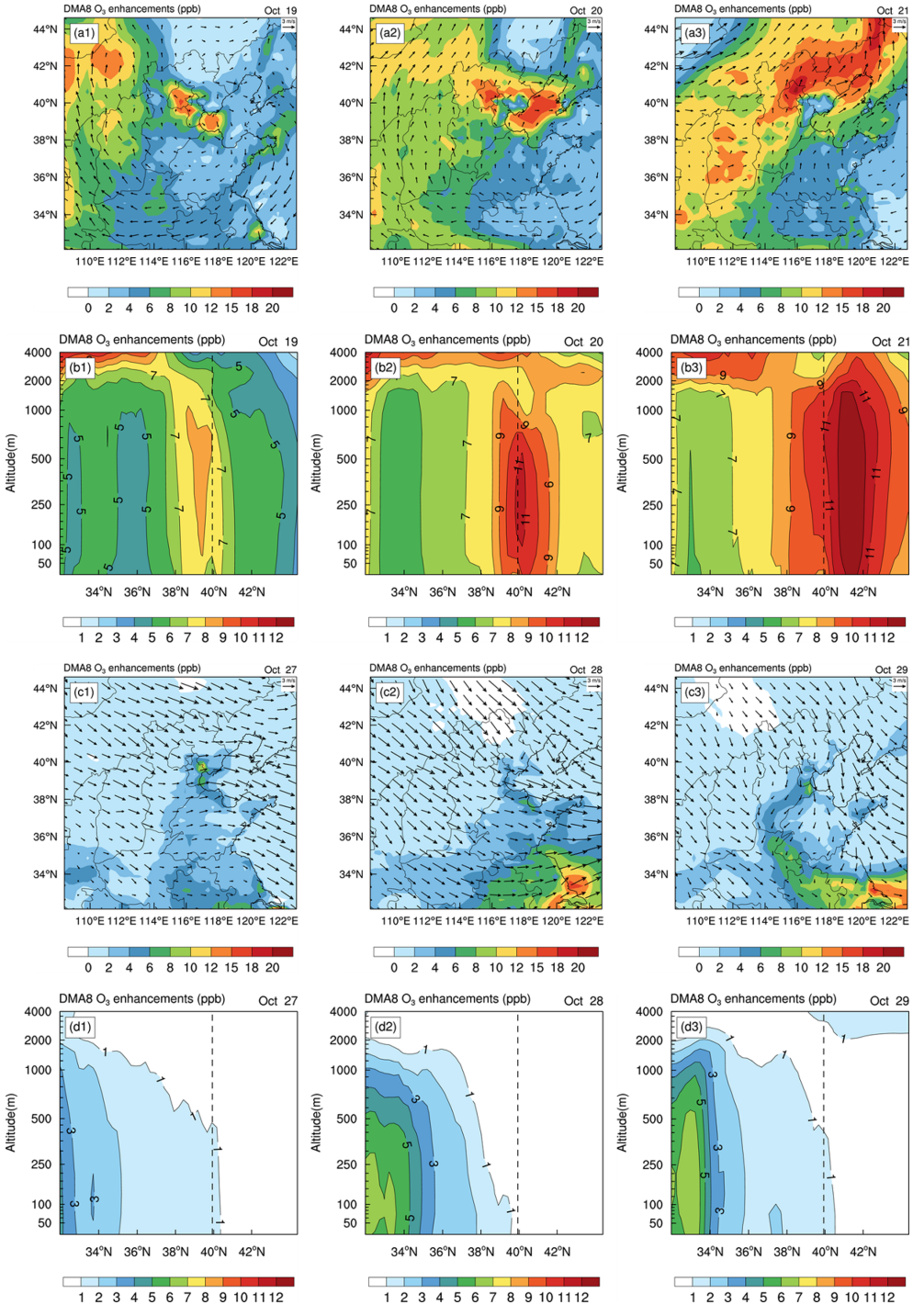

Figure 5. Surface-averaged (**a1–a3**, **c1–c3**) and zonal-averaged (**b1–b3**, **d1–d3**) DMA8 O_3 enhancements due to the six potential HONO sources in the North China Plain during a typical haze-aggravating process (19–21 October 2018) and a clean period (27–29 October 2018). The dashed line denotes the latitude of the BUCT site.

cant enhancement on regional HONO and secondary pollutants in crop-growing seasons.

The comparison of HONO concentrations/enhancements during a haze-aggravating process and a clean period is shown in Figs. 7 and 8. Generally, daytime HONO concentrations increased during haze-aggravating processes and were higher than concentrations on clean days. Het_{ground} was the dominant source of the surface HONO on both hazy and clean days and contributed 80 %–90 % of daytime averaged HONO concentrations (Fig. 8); however, this reac-

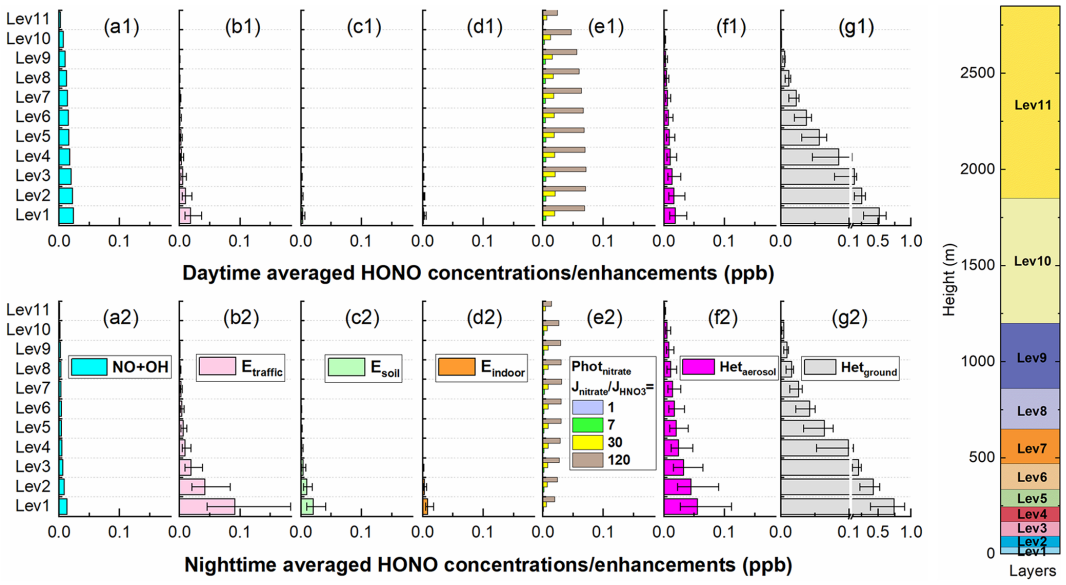

Figure 6. The 95-site-averaged daytime/nighttime HONO concentrations/enhancements at different heights for the NO + OH reaction (**a1** and **a2**) and each of the six potential HONO sources (**b1–g1** and **b2–g2**) during 11–31 October 2018. The error bar denotes the uncertainties of each potential HONO source in HONO concentrations (Table 2). The right panel denotes the approximate height of each vertical layer above the ground.

tion occurred only on the ground surface, thus its relative contribution decreased with height, especially during haze-aggravating processes (Fig. 8). Although the contribution of the NO + OH reaction to daytime HONO was small near the surface, its relative contribution to HONO increased with height, especially on clean days (Fig. 8). As for $Phot_{nitrate}$, a much larger enhancement was found on hazy days compared with clean days. On clean days the daytime enhanced HONO by $Phot_{nitrate}$ was only 1–3 ppt in general, and its contribution to daytime HONO was usually $<10\,\%$. During the haze-aggravating process, however, the enhanced HONO concentration by $Phot_{nitrate}$ was about 10 times higher than that on clean days and $Phot_{nitrate}$ became the dominant HONO source ($\sim 30\,\%$–$70\,\%$) at higher altitude, and both HONO concentrations and contributions by $Phot_{nitrate}$ increased with the air pollution aggravation (Figs. 7a–c, 8a–c). The contributions of direct emission sources were small and decreased when $PM_{2.5}$ increased, compared with the heterogeneous reactions. Higher concentrations of NO_2, nitrate, and $PM_{2.5}$ favored heterogeneous formation of HONO, while direct emission sources were relatively invariable under different pollution levels.

Our results show that nitrate concentrations increased with the haze-aggravating processes (Fig. 2b), and as a positive feedback effect, the elevated nitrate could in turn enhance HONO formation and further enhance the atmospheric oxidation capacity during daytime. Considering $J_{nitrate}$ is still unclear, sensitivity tests were conducted and are presented in the discussion section.

3.3.2 Enhanced OH and its production rate

Figure 9 demonstrates daytime variations in OH production (P(OH)) and loss (L(OH)) rates near the surface and in the vertically averaged layer (from the ground to a height of 2.5 km) at the 95 NCP sites for the Base and 6S cases during 11–31 October 2018. A significant enhancement of P/L(OH) can be found near the surface and vertically; the six potential HONO sources accelerated OH production and loss rates remarkably near the surface and noticeably in the vertical layers considered.

Near the surface, daytime P(OH) and L(OH) were significantly enhanced by $\sim 320\,\%$ for the 6S case (mean was 5.27 ppb h^{-1}) compared with the base case (mean was 1.26 ppb h^{-1}). For the base case, the daytime P(OH) via the photolysis of HONO and O_3 was 0.09 and 0.09 ppb h^{-1}, respectively, while the daytime L(OH) via the NO + OH reaction was 0.11 ppb h^{-1}, and the net contribution of HONO photolysis to P(OH) was -0.02 ppb h^{-1}. After adding the six potential HONO sources in case 6S, the daytime P(OH) via the photolysis of HONO and O_3 was 1.81 and 0.10 ppb h^{-1}, respectively, the daytime L(OH) via the NO + OH reaction was 0.48 ppb h^{-1}, and the net contribution of HONO photolysis to P(OH) reached 1.33 ppb h^{-1}. HONO photolysis was the main source of the primary formation of OH, while the secondary formed OH via the reaction of HO_2+NO (3.14 ppb h^{-1}) was the dominant source of the total OH formation.

Vertically, daytime P(OH) or L(OH) was enhanced by $\sim 105\,\%$ for the 6S case (mean was 2.21 ppb h^{-1}) compared

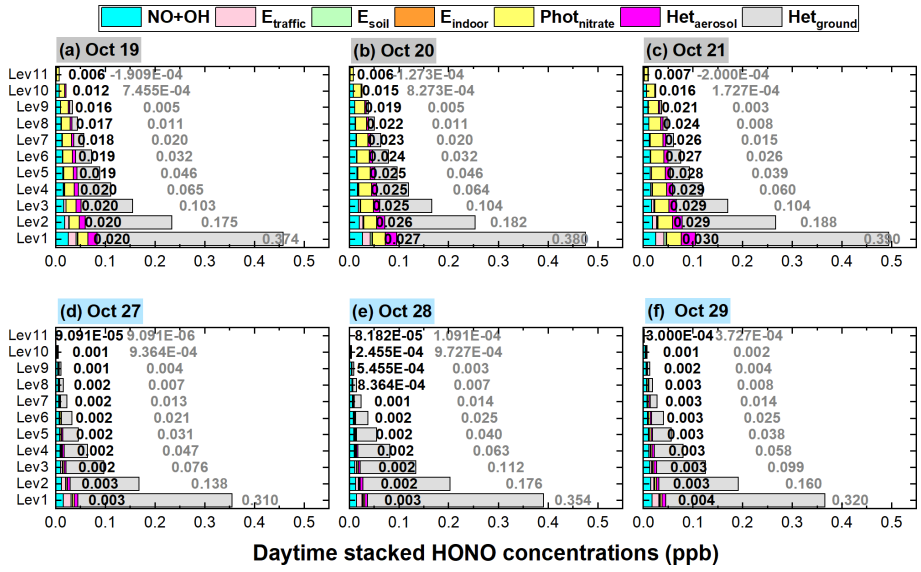

Figure 7. The 95-NCP-site-averaged daytime HONO concentrations at different heights when the NO + OH reaction and the six potential HONO sources were included for a typical haze-aggravating process during 19–21 October **(a–c)** and a clean period during 27–29 October 2018 **(d–f)**. The numbers in black in the first column of each graph are for $Phot_{nitrate}$, and the numbers in gray in the second column are for Het_{ground}.

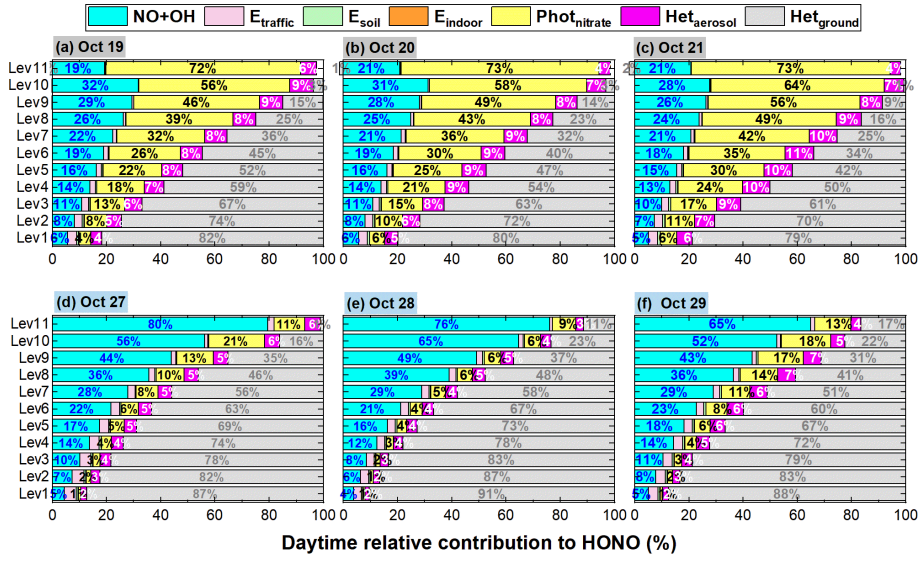

Figure 8. The 95-NCP-site-averaged relative contributions of the NO + OH reaction and each of the six potential HONO sources to daytime HONO concentrations at different heights for a typical haze-aggravating process during 19–21 October **(a–c)** and a clean period during 27–29 October 2018 **(d–f)**. The numbers in blue in the first column of each graph are for the NO + OH reaction, the numbers in black in the second column are for $Phot_{nitrate}$, the numbers in white in the third column are for $Het_{aerosol}$, and the numbers in gray in the fourth column are for Het_{ground}).

with the base case (mean was 1.08 ppb h^{-1}). For the base case, the daytime $P(OH)$ via the photolysis of HONO and O_3 was 0.06 and 0.10 ppb h^{-1}, respectively, while the daytime $L(OH)$ via the NO + OH reaction was 0.07 ppb h^{-1}, and the net contribution of HONO photolysis to $P(OH)$ was −0.01 ppb h^{-1}. After coupling the six potential HONO sources in case 6S, the daytime $P(OH)$ via the photolysis of HONO and O_3 and via the HO_2 + NO reaction was 0.48, 0.12 and 1.52 ppb h^{-1}, respectively, the daytime $L(OH)$ via the NO + OH reaction was 0.15 ppb h^{-1}, and the net contribution of HONO photolysis to $P(OH)$ was 0.33 ppb h^{-1}.

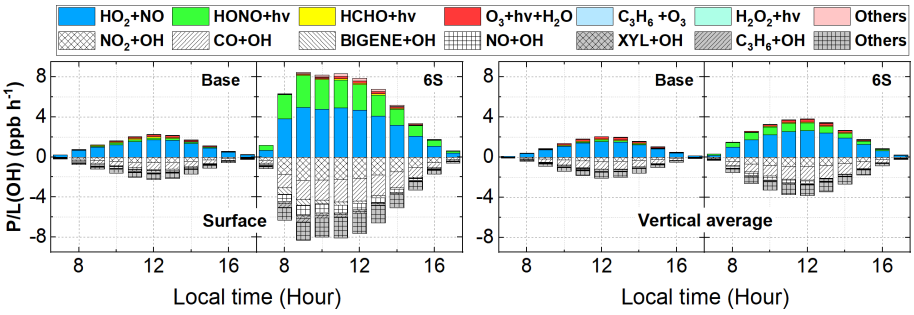

Figure 9. Diurnal mean variations in OH production (P(OH)) and loss (L(OH)) rates including major production and loss reactions near the surface and in the vertically averaged layer (from the ground to a height of 2.5 km) at the 95 NCP sites for the Base and 6S cases during 11–31 October 2018.

Figure 10 shows the linear relationships between daytime-averaged P(OH) and $PM_{2.5}$ concentrations and between daytime-averaged OH and $PM_{2.5}$ concentrations from the ground to a height of 2.5 km at the 95 NCP sites during 11–31 October 2018. Both P(OH) for the two cases (Base and 6S) and the enhanced P(OH) due to the six potential HONO sources showed a strong positive correlation ($r>0.8$) with $PM_{2.5}$ concentrations at the 95 NCP sites, because $Het_{aerosol}$, Het_{ground}, and $Phot_{nitrate}$ were significantly increased with the elevated pollution level. The enhanced P(OH) for the 6S case reached 0.043 ppb h^{-1} per 1 µg m^{-3} of a $PM_{2.5}$ enhancement. Similarly, a high positive correlation ($r>0.6$) was found between OH and $PM_{2.5}$ concentrations; the OH concentrations and enhancements due to the six potential HONO sources were both higher on hazy days than those on clean days, and the enhancement of OH reached 3.62×10^4 molec cm^{-3} per 1 µg m^{-3} of $PM_{2.5}$ for case 6S. These results are consistent with a recent field study reported by Slater et al. (2020), who found that the OH observed in haze events was elevated in central Beijing during November–December 2016. Furthermore, two observations confirmed the key role of HONO in producing primary OH despite the relatively lower photolysis frequency in haze-aggravating processes (Slater et al., 2020; Tan et al., 2018), consistent with our simulations (Fig. S7 shows the relationship between surface $PM_{2.5}$ and photolysis frequencies of NO_2, HONO, and HNO_3 in this study).

Figures 11 and 12 show detailed comparisons of P(OH) and OH enhancements during a haze-aggravating process and a clean period. It can be seen that both P(OH) and OH were enhanced on hazy days compared with clean days, and P(OH) and OH increased with the aggravated haze pollution. Among the six potential HONO sources, Het_{ground} was the largest contributor to the enhanced P(OH) and OH near the surface, but its contribution was relatively stable under different pollution levels and was rapidly reduced with height on both hazy and clean days; the contribution induced by $Phot_{nitrate}$ was remarkably increased in haze-aggravating processes and was about 10 times higher than that on clean days; $Het_{aerosol}$ also increased with the pollution levels but with relatively small values, while the impact of other three direct emission sources of HONO was quite small.

3.4 Enhanced DMA8 O_3

Figure 13 demonstrates the linear relationship between DMA8 O_3 enhancements and daytime $PM_{2.5}$ concentrations in each vertical layer and the averaged vertical layer for the 11 layers considered at the 95 NCP sites during 11–31 October 2018. A good correlation ($r>0.8$) between DMA8 O_3 enhancements and daytime $PM_{2.5}$ concentrations in the vertical averaged layer (similar reasons for the strong positive correlation between the enhanced P(OH) and $PM_{2.5}$ concentrations shown above) suggests that the enhanced O_3 due to the six potential HONO sources was larger on polluted days and increased during the haze-aggravating processes. The enhanced DMA8 O_3 was <2 ppb when $PM_{2.5}$ was <20 µg m^{-3} and was >10 ppb when $PM_{2.5}$ was >60 µg m^{-3} on average, with a mean DMA8 O_3 enhancement of 0.24 ppb per 1 µg m^{-3} of $PM_{2.5}$.

Figure 14 shows the 95-NCP-site-averaged DMA8 O_3 enhancements due to the six potential HONO sources for a typical haze-aggravating process during 19–21 October and a clean period during 27–29 October 2018. A significant enhancement of DMA8 O_3 can be found during the haze-aggravating process compared with that during clean days. The enhanced DMA8 O_3 was ~5.5 ppb (19 October), ~7 ppb (20 October), and ~10 ppb (21 October), during the haze-aggravating process, while it was usually ~2 ppb on clean days.

On clean days, Het_{ground} was the dominant contributor (~1.5–2 ppb) to the enhanced DMA8 O_3 among the six potential HONO sources; the contribution of $Phot_{nitrate}$ to the enhanced DMA8 O_3 was ~0.1–0.4 ppb, while that of the other four sources was minor. In the comparison between the haze-aggravating process (19–21 October) and clean days, the DMA8 O_3 enhancements induced by Het_{ground} were doubled and reached ~3–4 ppb; the contribution of $Phot_{nitrate}$ to the enhanced DMA8 O_3 substantially increased and reached ~2–4.5 ppb (19 October), ~3–6 ppb (20 Oc-

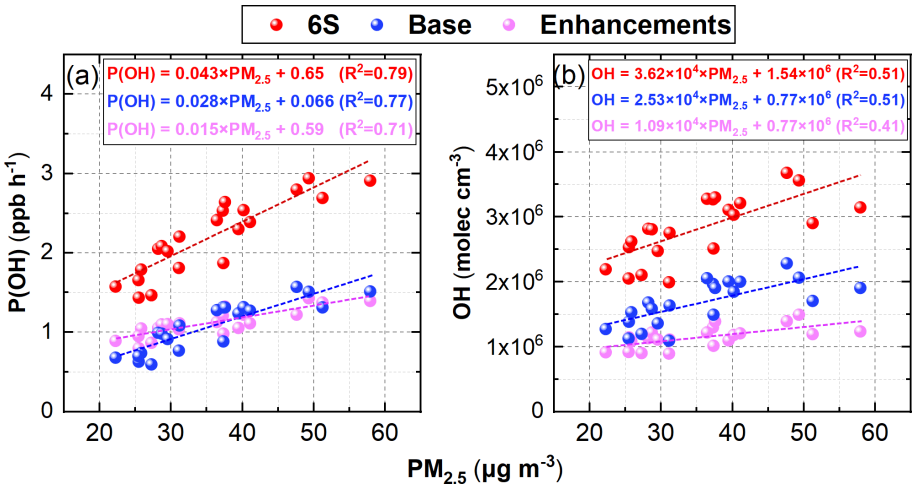

Figure 10. The linear relationships between daytime-averaged $P(\mathrm{OH})$ and $PM_{2.5}$ concentrations **(a)** and between daytime-averaged OH and $PM_{2.5}$ concentrations **(b)** from the ground to a height of 2.5 km at the 95 NCP sites during 11–31 October 2018.

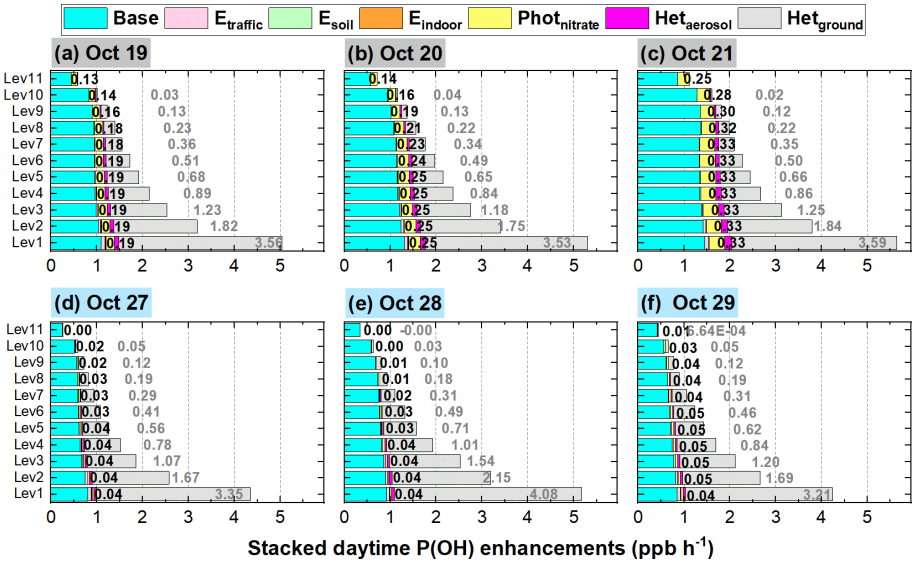

Figure 11. The 95-NCP-site-averaged daytime $P(\mathrm{OH})$ for the base case and the enhancements due to the six potential HONO sources for a typical haze-aggravating process during 19–21 October **(a–c)** and a clean period during 27–29 October 2018 **(d–f)**. The numbers in black in the first column of each graph are for $Phot_{nitrate}$, and the numbers in gray in the second column are for Het_{ground}.

tober),and ∼5–10 ppb (21 October). $Het_{aerosol}$ showed an increasing contribution to the enhanced DMA8 O_3 during the haze-aggravating process (∼0.3 ppb on 19 October, ∼0.4 ppb on 20 October, and ∼0.7 ppb on 21 October), while the impacts of the other three direct emission sources ($E_{traffic}$, E_{soil}, and E_{indoor}) on the enhanced DMA8 O_3 were minor.

3.5 Vertical variations of O_3-NO_x-VOC sensitivity

Based on the results presented in the previous section, $Phot_{nitrate}$ significantly enhanced the DMA8 O_3 10-fold in the vertical layers considered (especially at elevated heights) during polluted events, although previous studies have not fully discussed this. To better understand its role in vertical O_3 formation, the O_3-NO_x-VOC sensitivity was analyzed by using the $P(H_2O_2)/P(HNO_3)$ ratio proposed by Sillman (1995), which is more suitable than the concentration ratio of H_2O_2/HNO_3 because of the large dry deposition velocity of the two gases in the troposphere (Sillman, 1995). A transition point of $P(H_2O_2)/P(HNO_3) = 0.35$ was suggested by Sillman (1995); when $P(H_2O_2)/P(HNO_3)$ was <0.35, O_3 shows VOC-sensitive chemistry (increasing VOC concentrations can significantly elevate O_3 levels) and when $P(H_2O_2)/P(HNO_3)$ was >0.35, O_3 tends to NO_x-sensitive

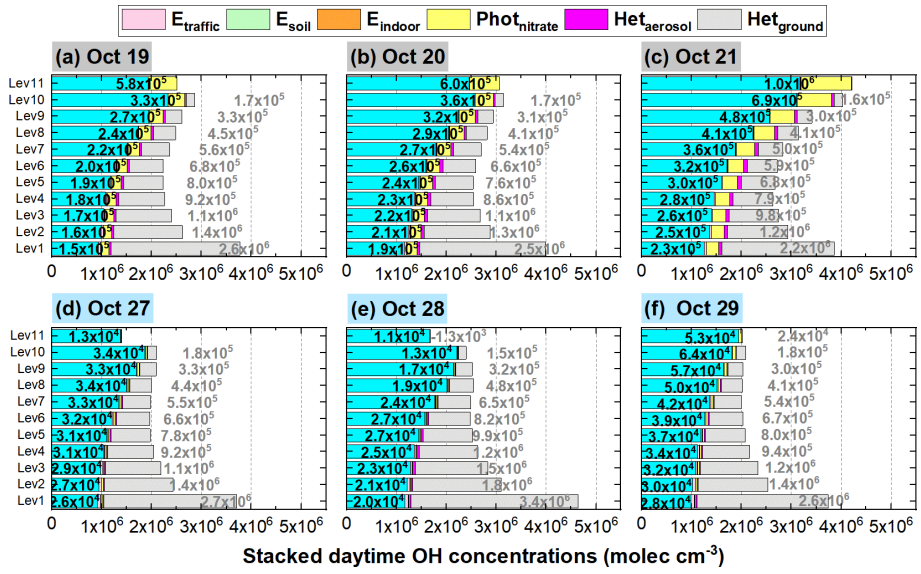

Figure 12. The 95-NCP-site-averaged daytime OH concentrations for the base case and the enhancements due to the six potential HONO sources for a typical haze-aggravating process during 19–21 October **(a–c)** and a clean period during 27–29 October 2018 **(d–f)**. The numbers in black in the first column of each graph are for $Phot_{nitrate}$, and the numbers in gray in the second column are for Het_{ground}.

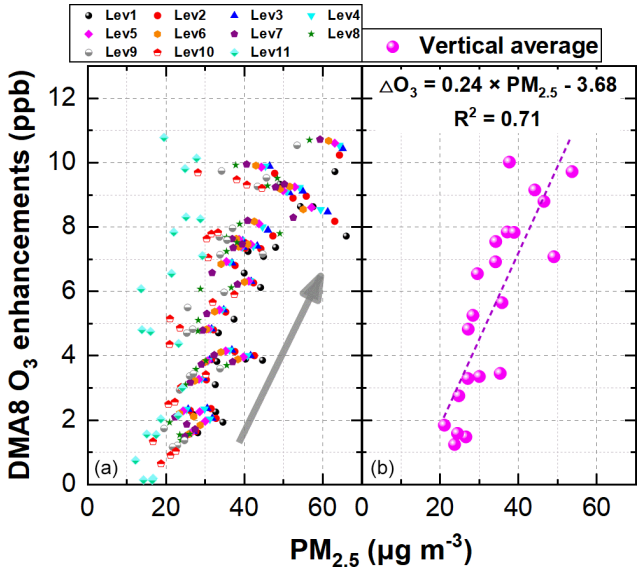

Figure 13. The linear relationship between DMA8 O_3 enhancements and daytime $PM_{2.5}$ concentrations in each vertical layer **(a)** and the averaged vertical layer for the 11 layers considered **(b)** at the 95 NCP sites during 11–31 October 2018.

chemistry (increasing NO_x concentrations can significantly elevate O_3 levels).

Figure 15 demonstrates the 95-NCP-site-averaged $P(H_2O_2)/P(HNO_3)$ ratio at each vertical layer for the 6S case for a typical haze-aggravating process during 19–21 October and a clean period during 27–29 October 2018. A clearly opposite O_3 sensitivity appeared between the lower layers (VOC sensitive) and the higher layers (NO_x sensitive) on both clean and hazy days, and the transition point usually appeared at the eighth layer (~ 600–800 m).

The $Phot_{nitrate}$ reaction is assumed to produce HONO and NO_x (Zhou et al., 2003; Romer et al., 2018; Gen et al., 2022). This reaction not only enhances OH concentrations via HONO photolysis, but also directly releases NO_x back into the troposphere. Considering the NO_x-sensitive O_3 chemistry at higher layers (>800 m), elevating OH and NO_x concentrations are both favorable for O_3 formation, especially in haze-aggravating processes with abundant nitrate (detailed vertically enhanced O_3 production/loss rates induced by $Phot_{nitrate}$ are shown in Fig. S8).

The specific role of the HONO or NO_2 produced via the $Phot_{nitrate}$ reaction (Reaction R2) in DMA8 O_3 enhancements was further analyzed and is shown in Fig. 16. The produced NO_2 and HONO jointly promoted O_3 formation and increased DMA8 O_3 concentrations. From the surface to ~ 1200 m (Level 9), the DMA8 O_3 enhancements for case D_HONO was ~ 5 times those for case D_NO_2, while at ~ 2000 m (Level 11) the DMA8 O_3 enhancements for case D_HONO was ~ 2 times those for case D_NO_2. A balance exists between the propagation of the free radical interconversion cycle and the rate of termination of the cycle for the O_3 formation chemistry (Gligorovski et al., 2015). Considering the 0.67 and 0.33 yields (ratio of 2) for the two products, we could conclude that the impact of produced HONO on O_3 enhancements was larger than that of produced NO_2 near the surface, while at higher altitude (>2000 m) the impacts of the two products were similar.

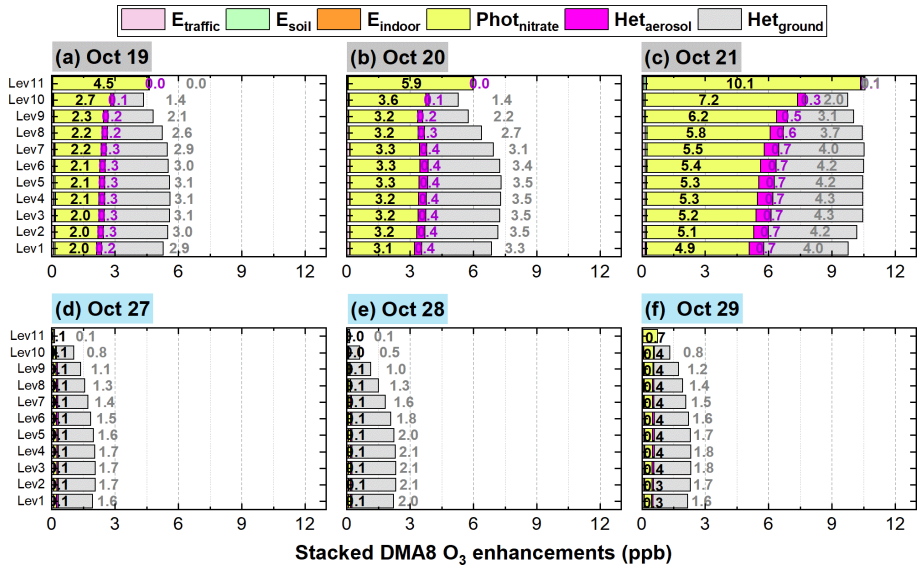

Figure 14. The 95-NCP-site-averaged DMA8 O_3 enhancements due to the six potential HONO sources for a typical haze-aggravating process during 19–21 October **(a–c)** and a clean period during 27–29 October 2018 **(d–f)**. The numbers in black in each graph are for $Phot_{nitrate}$, the numbers in purple are for $Het_{aerosol}$, and the numbers in gray are for Het_{ground}.

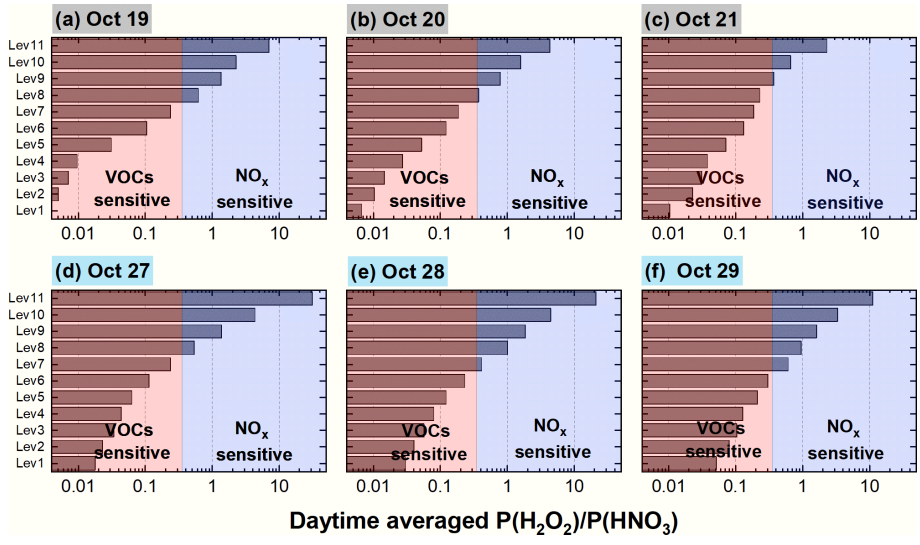

Figure 15. The 95-NCP-site-averaged $P(H_2O_2)/P(HNO_3)$ ratio at each vertical layer for the 6S case for a typical haze-aggravating process during 19–21 October **(a–c)** and a clean period during 27–29 October 2018 **(d–f)**.

4 Discussion

4.1 Vertical variations of potential HONO sources

The relative contribution of potential HONO sources near the surface, corresponding to the first model layer (0 to ~35 m) in our simulation, was quantified in previous modeling studies (Fu et al., 2019; Xue et al., 2020; Zhang et al., 2021); however, for those potential HONO sources, their relative contributions to HONO concentrations near and above the surface should be different. Based on our results (Figs. 7 and 8), the effects of aerosol-related HONO sources would be severely underestimated on hazy days when only focused on surface HONO, especially for $Phot_{nitrate}$. Near the surface in NCP, the daytime contribution of $Phot_{nitrate}$ to HONO concentrations on hazy days was only ~4 %–6 %, but this source contributed ~35 %–50 % of the enhanced DMA8 O_3 (Fig. 14a–c); above the eighth layer (~800 m), this source contributed ~50 %–70 % of HONO concentrations and ~50 %–95 % of the enhanced DMA8 O_3 (Fig. 14a–c).

A recent observation in urban Beijing reported vertical HONO concentrations from three heights above the ground

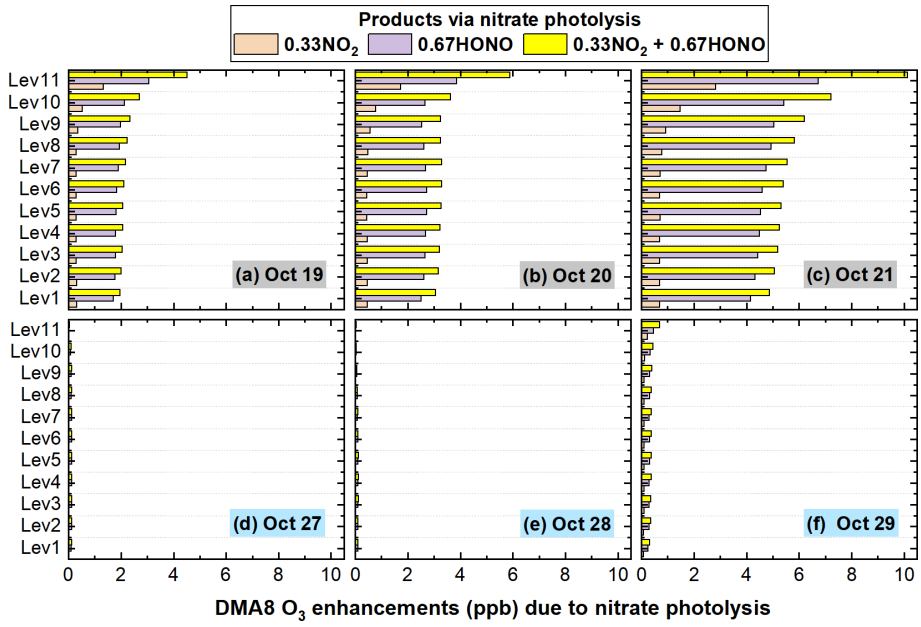

Figure 16. The 95-NCP-site-averaged DMA8 O_3 enhancements due to nitrate photolysis with three product scenarios (cases D_NO_2, D_HONO and D) for a typical haze-aggravating process during 19–21 October **(a–c)** and a clean period during 27–29 October 2018 **(d–f)**.

and found that extremely high HONO concentrations occurred at 120 m (∼ 5 ppb) and 240 m (∼ 3 ppb) rather than near the surface (∼ 1.2 ppb) during 12:00 on a typical hazy day (W. Q. Zhang et al., 2020). The observation was unusual at noontime under strong convection conditions, inconsistent with those during most of the previous observations indicating a HONO decreasing trend with height, especially with the observational results of Zhu et al. (2011) and Meng et al. (2020) as well as the simulated results of Zhang et al. (2021) and our results in Fig. S6 at the same observational site. The contributions of different HONO sources at each layer were analyzed by using a box model, but ∼ 80 %–90 % of the noontime HONO at higher layers could not be explained by the known HONO formation mechanisms (W. Q. Zhang et al., 2020). The box model neglected the vertical convection, and thus the ground-related HONO sources had no contribution to HONO concentrations at the higher layers; therefore, their HONO simulations were actually underestimated compared with our results and those from the studies by Wong et al. (2011) and Zhang et al. (2021).

4.2 Uncertainties of $J_{nitrate}/J_{HNO_3}$ ratios and their impacts

4.2.1 Uncertainties of $J_{nitrate}/J_{HNO_3}$ ratios in DMA8 O_3 enhancements

Based on our results, Het_{ground} and $Phot_{nitrate}$ were the two major contributors to the enhanced DMA8 O_3, especially for $Phot_{nitrate}$ on hazy days with higher $PM_{2.5}$ concentrations. The uncertainties of $Phot_{nitrate}$ (four $J_{nitrate}/J_{HNO_3}$ ratios) in O_3 enhancements were analyzed and are shown in Fig. 17 (The uncertainties of Het_{ground} are presented in Sect. S2). During the haze-aggravating process, the enhanced DMA8 O_3 near the surface increased from ∼ 0.3 to ∼ 0.5 ppb, from ∼ 0.9 to ∼ 2 ppb, from ∼ 2 to ∼ 6 ppb, and from ∼ 5 to ∼ 12 ppb, with the $J_{nitrate}/J_{HNO_3}$ ratio being 1, 7, 30, and 120, respectively, and the enhanced O_3 increased with altitude. On clean days, the impact of $Phot_{nitrate}$ on O_3 enhancements was small (<1 ppb) even with a $J_{nitrate}/J_{HNO_3}$ ratio of 120.

4.2.2 Uncertainties of $J_{nitrate}/J_{HNO_3}$ ratios in nitrate concentrations

We found considerable enhancements in O_3 concentrations induced by $Phot_{nitrate}$, yet it is still unclear that to what extent $Phot_{nitrate}$ could influence nitrate concentrations. The overall nitrate concentrations for the base case and the nitrate enhancements induced by the potential HONO sources decreased with rising altitude except for $Phot_{nitrate}$ (Fig. S9a). Het_{ground} enhanced nitrate concentrations by ∼ 1.5 μg m^{-3} near the surface and the enhancements decreased to <0.5 μg m^{-3} above the eighth model layer (∼ 800 m); the nitrate enhancements due to $Het_{aerosol}$ and $E_{traffic}$ near the surface were ∼ 0.2 and ∼ 0.1 μg m^{-3}, respectively, and were <0.1 and <0.04 μg m^{-3} above the sixth model layer (∼ 500 m). For $Phot_{nitrate}$, the overall impact of four $J_{nitrate}/J_{HNO_3}$ ratios on nitrate concentrations is shown in Fig. S9b; a smaller $J_{nitrate}/J_{HNO_3}$ ratio of 1 or 7 had a limited impact on nitrate concentrations of ∼ 0–0.05 μg m^{-3}, a $J_{nitrate}/J_{HNO_3}$ ratio of 30 slightly decreased nitrate con-

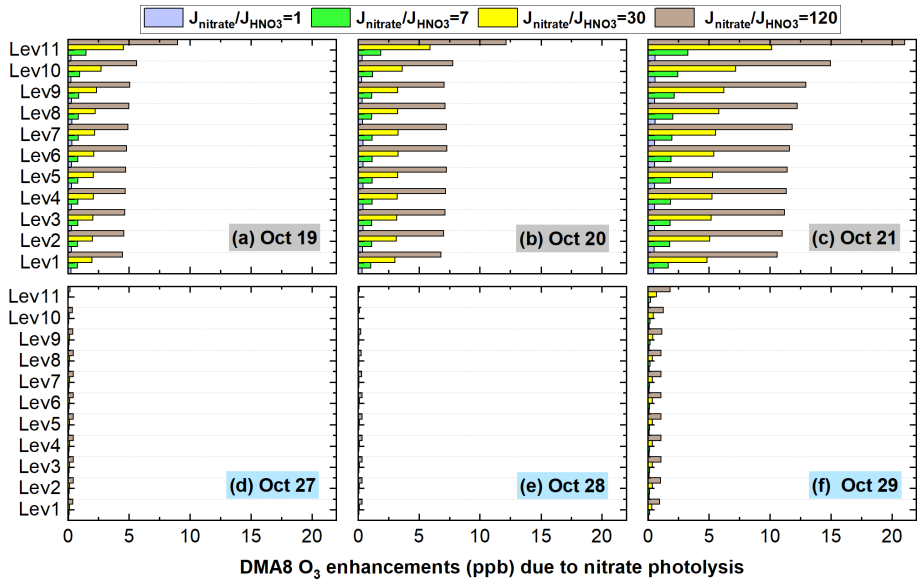

Figure 17. The 95-NCP-site-averaged DMA8 O_3 enhancement induced by nitrate photolysis with four $J_{nitrate}/J_{HNO_3}$ ratios (1, 7, 30, and 120) for a typical haze-aggravating process during 19–21 October **(a–c)** and a clean period during 27–29 October 2018 **(d–f)**.

centrations by $\sim 0.2\,\mu g\,m^{-3}$, while the $J_{nitrate}/J_{HNO_3}$ ratio of 120 decreased vertical nitrate concentrations by ~ 0.3–$0.8\,\mu g\,m^{-3}$. The relative nitrate changes caused by $Phot_{nitrate}$ were calculated by the differences between four cases of added $Phot_{nitrate}$ (cases Nit_1, Nit_7, D, and Nit_120) and the base case (Fig. S9c). The vertical nitrate concentrations were reduced by $\sim 0\,\%$–$0.4\,\%$ ($J_{nitrate}/J_{HNO_3} = 1$), $\sim 0\,\%$–$2\,\%$ (7), $\sim 2\,\%$–$5\,\%$ (30), and $\sim 10\,\%$–$14\,\%$ (120) at the 95 NCP sites, meaning that the $Phot_{nitrate}$ impact on vertical nitrate concentrations is limited ($<5\,\%$) when adopting a relatively small $J_{nitrate}/J_{HNO_3}$ ratio (<30) (Fig. S9c).

Romer et al. (2018) found a $J_{nitrate}/J_{HNO_3}$ ratio of 10 or 30 had a much larger effect on HONO than on HNO_3, and $Phot_{nitrate}$ accounted for an average of 40 % of the total production of HONO, and only 10 % of HNO_3 loss with a $J_{nitrate}/J_{HNO_3}$ ratio of 10 (Fig. 5 in Romer et al., 2018), consistent with our study. From the production rate of gas HNO_3 (P_{HNO_3}) in Fig. S10, we find that an increase in the $J_{nitrate}/J_{HNO_3}$ ratio for $Phot_{nitrate}$ simultaneously enhances the HNO_3 production rate, and is favorable for nitrate formation via the reaction between HNO_3 and NH_3. Nitrate consumption is mitigated by the faster nitrate formation, and this is the main reason for less perturbation of the nitrate budget influenced by $Phot_{nitrate}$.

Figure 18 shows the detailed relative changes of nitrate caused by $Phot_{nitrate}$ during a typical haze-aggravating process and a clean period (corresponding concentrations are shown in Fig. S11). The percentage nitrate reduction was usually smaller on hazy days than on clean days, mainly due to the slightly weaker photolysis frequency during pollution events (Fig. S7). The nitrate reduction was $<5\,\%$ when adopting a $J_{nitrate}/J_{HNO_3}$ ratio of 30 on both clean and hazy days and was $<15\,\%$ in most cases even when the $J_{nitrate}/J_{HNO_3}$ ratio reached 120.

4.2.3 Possible ranges of the $J_{nitrate}/J_{HNO_3}$ ratio

From the above discussion, we find that the enhanced OH and O_3 due to $Phot_{nitrate}$ are significant during haze-aggravating processes, and the exact value of the $J_{nitrate}/J_{HNO_3}$ ratio requires more study.

Figure 19 shows the diurnal patterns of surface-averaged and vertically averaged simulations of the $Phot_{nitrate}$ frequency with four different $J_{nitrate}/J_{HNO_3}$ ratios at the 95 NCP sites during the study period. The $Phot_{nitrate}$ frequency at 12:00 was 3.7×10^{-7}, 2.6×10^{-6}, 1.1×10^{-5}, and $4.5 \times 10^{-5}\,s^{-1}$ when adopting a $J_{nitrate}/J_{HNO_3}$ ratio of 1, 7, 30, and 120, respectively. The corresponding vertically averaged $Phot_{nitrate}$ frequency was slightly larger ($\sim 10\,\%$) and was 4.2×10^{-7}, 2.9×10^{-6}, 1.3×10^{-5}, and $5.0 \times 10^{-5}\,s^{-1}$, respectively. Adopting a $J_{nitrate}/J_{HNO_3}$ ratio of 30 in the 6S case, with the corresponding $J_{nitrate}$ of 1.1–$1.3 \times 10^{-5}\,s^{-1}$, produced $\sim 30\,\%$–$50\,\%$ of the enhanced O_3 near the surface on hazy days (Fig. 14), and $\sim 70\,\%$–$90\,\%$ of the enhanced O_3 at higher layers ($>800\,m$).

The reported values of $J_{nitrate}$ from previous studies are summarized in Table 4. The experimental $J_{nitrate}$ values have been controversial over the past two decades and are still being debated. In our simulations for the 6S case, $Phot_{nitrate}$ contributed from $\sim 1\,\%$ (clean days) to $\sim 5\,\%$ (hazy days) to surface HONO during daytime when using the $J_{nitrate}/J_{HNO_3}$ ratio of 30 in NCP, consistent with $<8\,\%$ at a rural site in NCP reported by Xue et al. (2020) and $\sim 1\,\%$ in urban Beijing reported by Zhang et al. (2021) using the same

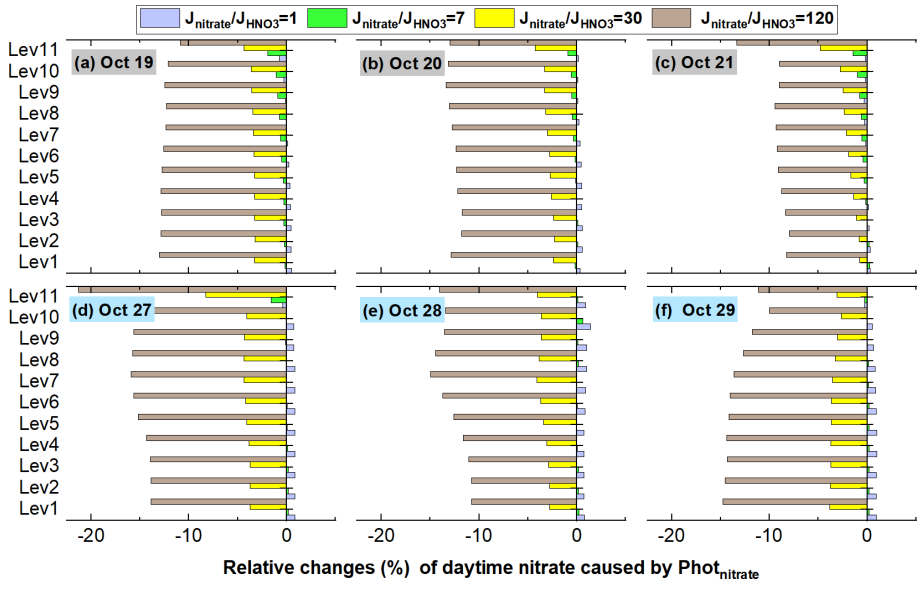

Figure 18. The 95-NCP-site-averaged relative changes of nitrate with four $J_{\mathrm{nitrate}}/J_{\mathrm{HNO_3}}$ ratios (1, 7, 30, and 120) compared with the base case for a typical haze-aggravating process during 19–21 October **(a–c)** and a clean period during 27–29 October 2018 **(d–f)**.

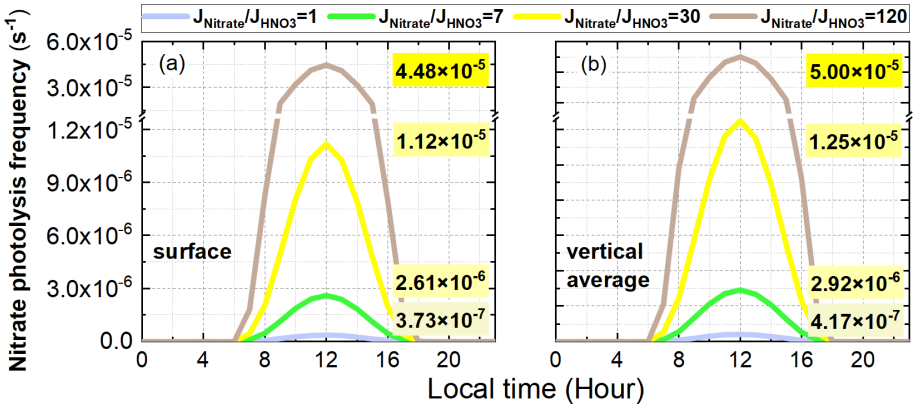

Figure 19. Diurnal patterns of surface-averaged **(a)** and vertically averaged **(b)** simulations of the nitrate photolysis frequency with four different $J_{\mathrm{nitrate}}/J_{\mathrm{HNO_3}}$ ratios (1, 7, 30, 120) at the 95 NCP sites during the study period. The nitrate photolysis frequencies at 12:00 are shown in each graph.

ratio; however, the increasing contribution of $\mathrm{Phot_{nitrate}}$ to HONO concentrations with rising altitude based on our simulations (Figs. 7 and 8) has not been discussed in previous research. Furthermore, we found that the overall $\mathrm{Phot_{nitrate}}$ impact on OH and O_3 would be severely underestimated if the $\mathrm{Phot_{nitrate}}$ contribution to vertical HONO was excluded.

A larger $J_{\mathrm{nitrate}}/J_{\mathrm{HNO_3}}$ ratio of 120 for $\mathrm{Phot_{nitrate}}$ (4.5–$5.0 \times 10^{-5}\ \mathrm{s^{-1}}$ at 12:00) produced ∼25 %–30 % of noontime HONO in NCP in our study (Fig. S12), comparable to 30 %–40 % in previous modeling studies (Fu et al., 2019; Shi et al., 2020) when using the $J_{\mathrm{nitrate}}/J_{\mathrm{HNO_3}}$ ratio of 118.57 ($8.3 \times 10^{-5}/7 \times 10^{-7}$). In haze-aggravating processes, the contribution of $\mathrm{Phot_{nitrate}}$ ($J_{\mathrm{nitrate}}/J_{\mathrm{HNO_3}} = 120$) to the DMA8 O_3 enhancements reached ∼5–10 ppb near the surface and ∼8–20 ppb above the 10th model layer (Fig. 17), these enhancements were extremely large. In a previous modeling study by Fu et al. (2020), the daytime surface O_3 simulations were systematically overestimated by ∼5 ppb in NCP in winter (Fig. S4 in Fu et al., 2020); the inclusion of $\mathrm{Phot_{nitrate}}$ ($J_{\mathrm{nitrate}}/J_{\mathrm{HNO_3}} = 118.57$) in their study might have caused the overestimation. From the above, a $J_{\mathrm{nitrate}}/J_{\mathrm{HNO_3}}$ ratio of 120 or a J_{nitrate} value of $\sim 4\text{–}5 \times 10^{-5}\ \mathrm{s^{-1}}$ is possibly overestimated. When adopting the maximum J_{nitrate} value of $10^{-4}\ \mathrm{s^{-1}}$ reported by Ye et al. (2016a) and Bao et al. (2018), we reasonably speculate that O_3 simulations will be significantly overestimated, especially at higher altitude with NO_x-sensitive O_3 chemistry (Fig. 15).

Table 4. Summary of studies on the nitrate photolysis frequency ($J_{nitrate}$) (J_{HNO_3} denotes the photolysis frequency of gas HNO_3).

Experimental conditions	Main conclusion	Reference
HNO_3 absorbed on Pyrex surface	$J_{nitrate}$ (1.2×10^{-5} s^{-1}) is 1–2 orders of magnitude faster than in the gas and aqueous phases.	Zhou et al. (2003)
Atmosphere simulation chamber	$J_{nitrate}$ on snow, ground, and glass surfaces can be excluded in the chamber.	Rohrer et al. (2005)
HNO_3 absorbed on glass surface	Photolysis frequency of surfaces adsorbed HNO_3 is >2 orders of magnitude larger than J_{HNO_3}.	Zhu et al. (2008)
Urban grime-coated surface	$J_{nitrate}$ (1.2×10^{-3} s^{-1}) is 4 orders of magnitude faster than in water (10^{-7} s^{-1}).	Baergen and Donaldson (2013)
Various natural/artificial surfaces	$J_{nitrate}$ ranges from 6.0×10^{-6} to 3.7×10^{-4} s^{-1}, 1–3 orders of magnitude higher than J_{HNO_3}	Ye et al. (2016a)
Adsorbed HNO_3 on glass surfaces	Photolysis frequency of surfaces adsorbed HNO_3 (2.4×10^{-7} s^{-1}) is very low.	Laufs and Kleffmann (2016)
Aerosol filter samples	$J_{nitrate}$ ranges from 6.2×10^{-6} to 5.0×10^{-4} s^{-1} with a mean of 1.3×10^{-4} s^{-1}.	Ye et al. (2017)
Nitrate aerosol in the MBL	$J_{nitrate}$ is ∼ 10 times higher than J_{HNO_3}.	Reed et al. (2017)
$PM_{2.5}$ in Beijing	$J_{nitrate}$ (1.22×10^{-5} to 4.84×10^{-4} s^{-1}) is 1–3 orders of magnitude higher than J_{HNO_3}.	Bao et al. (2018)
Sea-salt particulate nitrate	$J_{nitrate}$ is 25–50 times higher than J_{HNO_3}.	Kasibhatla et al. (2018)
Particles collected on filters	$J_{nitrate}$ is ≤ 30 times J_{HNO_3}.	Romer et al. (2018)
CMAQ simulation	Nitrate photolysis contributed ∼ 30 % of noontime HONO with a $J_{nitrate}/J_{HNO_3}$ ratio of ∼ 120.	Fu et al. (2019)
CMAQ simulation	A $J_{nitrate}/J_{HNO_3}$ ratio of 100 improved sulfate simulations better than a $J_{nitrate}/J_{HNO_3}$ ratio of 10.	Zheng et al. (2020)
MCM Box model	Nitrate photolysis contribution to HONO was <8 % with a $J_{nitrate}/J_{HNO_3}$ ratio of 30.	Xue et al. (2020)
MCM Box model	Nitrate photolysis contributed ∼ 40 % of noontime HONO with a $J_{nitrate}/J_{HNO_3}$ ratio of ∼ 120.	Shi et al. (2020)
Smog chamber	The $J_{nitrate}/J_{HNO_3}$ ratio was <10 for suspended submicron $NaNO_3$ and NH_4NO_3.	Shi et al. (2021)
CMAQ simulation	Nitrate photolysis contribution to surface HONO was ∼ 1.0 % with a $J_{nitrate}/J_{HNO_3}$ ratio of 30.	Zhang et al. (2021)
WRF-Chem simulation	The relative contribution of nitrate photolysis to HONO increased with rising altitude, and nitrate photolysis contributed to the enhanced O_3 much more in the ABL than near the surface. On average, nitrate photolysis contributed ∼ 5 % of surface daytime HONO with a $J_{nitrate}/J_{HNO_3}$ ratio of 30 (∼ 1×10^{-5} s^{-1}) but contributed ∼ 30 %–50 % of the enhanced O_3 near the surface in NCP on hazy days.	This study

MBL: marine boundary layer; ABL: atmospheric boundary layer.

Romer et al. (2018) and Kasibhatla et al. (2018) suggested that a $J_{nitrate}/J_{HNO_3}$ ratio of 30 or smaller would be more suitable, being about the minimum value reported by Ye et al. (2016a) and Bao et al. (2018). This ratio has shown significant influence on the O_3 simulations in haze-aggravating processes in this study. The lack of photo-catalyzer in suspended submicron particulate sodium and ammonium nitrate may cause a lower $J_{nitrate}/J_{HNO_3}$ ratio (<10), as reported by Shi et al. (2021), and thus more chamber experiments need to be conducted by using the particles collected in the real atmosphere. Choosing a larger $J_{nitrate}$ value might cover up other ground-based unknown HONO sources, creating an illusion of good model simulations of daytime HONO, but resulting in an overestimation of O_3 concentrations. Considering the uncertainties of NO_x or VOC emissions, which also significantly impact O_3 simulations, more studies are needed to find the exact value of $J_{nitrate}$ in the real atmosphere.

4.3 Interactions between heterogeneous HONO sources

Form the comparison of nitrate budget induced by the six potential HONO sources in Figs. S3 and S9, we find that Het_{ground} led to a significant increase in nitrate concentrations. In the real atmosphere, the NO_2 heterogeneous reactions and the $Phot_{nitrate}$ reaction occur simultaneously,

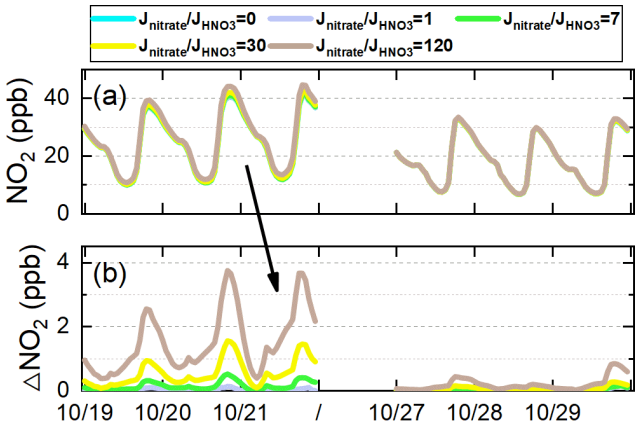

Figure 20. Comparison of 95-site-averaged simulations of NO_2 concentrations for the base case and four cases with different $J_{nitrate}/J_{HNO_3}$ ratios (1, 7, 30, and 120) **(a)**, and the corresponding NO_2 variations **(b)** compared with the base case in the North China Plain during 11–31 October 2018.

whereas the sensitivity tests considered only one specific HONO source for each case and neglected their interactions, leading to the underestimation of the $Phot_{nitrate}$ impact to some extent. When this is taken into consideration, the $Phot_{nitrate}$ impact on atmospheric oxidants and secondary pollutants would be even larger, especially during the haze-aggravating process.

$Phot_{nitrate}$ would in turn change NO_x concentrations to some extent. From the 95-site-averaged NO_2 concentrations shown in Fig. 20, we find that $Phot_{nitrate}$ slightly increased NO_2 concentrations on hazy days. The elevated NO_2 concentration could enhance HONO formation via the NO_2 heterogeneous reactions; nevertheless, due to the high background NO_2 concentrations in NCP (up to ~ 40 ppb at nighttime), the increment of NO_2 and the enhanced HONO formation from NO_2 caused by $Phot_{nitrate}$ were small (<10 %), but might have a larger impact on NO_x budgets in clean regions. From the above, a positive feedback relationship between the NO_2 heterogeneous reactions and the $Phot_{nitrate}$ reaction was found, and these multi-processes worsen the air quality during haze-aggravating processes.

5 Conclusions

In this study, three direct emission sources, the improved NO_2 heterogeneous reactions on aerosol and ground surfaces, and particulate nitrate photolysis in the atmosphere were included in the WRF-Chem model to explore the key HONO sources producing O_3 enhancements during typical autumn haze-aggravating processes with co-occurrence of high $PM_{2.5}$ and O_3 in NCP. The six potential HONO sources produced a significant enhancement in surface HONO simulations and improved the mean HONO concentration at the BUCT site to 1.47 ppb from 0.05 ppb (improved the NMB to −14.22 % from −97.11 % and the IOA to 0.80 from 0.45). The improved HONO significantly enhanced the atmospheric oxidation capacity near the surface and at elevated heights, especially on hazy days, resulting in rapid formation of and significant improvements in O_3 during haze-aggravating processes in NCP. Although the photolysis frequency is usually lower during hazy days, higher concentrations of NO_2, $PM_{2.5}$, and nitrate favored HONO formation via heterogeneous reactions, leading to stronger atmospheric oxidation capacity. The major results include:

1. For the surface HONO in NCP, Het_{ground} was the largest source during daytime and nighttime (~ 50 %–80 %); the contribution of $Phot_{nitrate}$ ($J_{nitrate}/J_{HNO_3} = 30$) to surface HONO concentrations was close to that of the NO + OH reaction during daytime (~ 1 %–12 %) and was ~ 5 % for daytime average; the contribution of $E_{traffic}$ was important during nighttime (~ 10 %–20 %) but small during daytime (<5 %); the contribution of $Het_{aerosol}$ was minor (~ 2 %–3 %) in the daytime and <10 % at nighttime; the contribution of E_{soil} was <3 %, and E_{indoor} could be neglected. Vertically, the HONO enhancements due to ground-based potential HONO sources ($E_{traffic}$, E_{soil}, E_{indoor}, and Het_{ground}) decreased rapidly with height, while the NO + OH reaction and aerosol-related HONO sources ($Phot_{nitrate}$ and $Het_{aerosol}$) decreased with height much slower. The enhanced HONO due to $Phot_{nitrate}$ on hazy days was about 10 times larger than on clean days and became the dominant HONO source (~ 30 %–70 % when $J_{nitrate}/J_{HNO_3} = 30$) at higher layers, and both HONO concentrations and $Phot_{nitrate}$ contributions increased with the aggravated pollution levels.

2. Near the surface, daytime OH production/loss rates were significantly enhanced by ~ 320 % for the 6S case (mean of 5.27 ppb h^{-1}) compared with the base case (mean of 1.26 ppb h^{-1}); vertically, daytime OH production/loss rates were enhanced by ~ 105 % for the 6S case (mean of 2.21 ppb h^{-1}) compared with the base case (mean of 1.08 ppb h^{-1}). The enhanced OH production rate and OH due to the six potential HONO sources both showed a strong positive correlation with $PM_{2.5}$ concentrations at the 95 NCP sites, with a slope of 0.043 ppb h^{-1} per 1 µg m^{-3} of $PM_{2.5}$ and 3.62×10^4 molec cm^{-3} per 1 µg m^{-3} of $PM_{2.5}$ from the surface to the height of 2.5 km for case 6S, respectively. The atmospheric oxidation capacity (e.g., OH) was enhanced in the haze-aggravating process.

3. A strong positive correlation ($r > 0.8$) between enhanced O_3 by the six potential HONO sources and $PM_{2.5}$ concentrations was found in NCP, and nitrate photolysis was the largest contributor to the enhanced DMA8 O_3 on hazy days. Vertically, the enhanced DMA8 O_3 was <2 ppb when $PM_{2.5}$ was <20 µg m^{-3}, and it

was >10 ppb when $PM_{2.5}$ was >60 µg m^{-3} on average, with a slope of 0.24 ppb DMA8 O_3 enhancement per 1 µg m^{-3} of $PM_{2.5}$. The surface-enhanced DMA8 O_3 was ∼5.5 ppb (19 October), ∼7 ppb (20 October), and ∼10 ppb (21 October) during a typical haze-aggravating process, while it was usually ∼2 ppb on clean days. The contribution of $Phot_{nitrate}$ to the enhanced DMA8 O_3 was increased by over 1 magnitude during the haze-aggravating process (up to 5–10 ppb) compared with that on clean days (∼0.1–0.5 ppb), and reached ∼2–4.5 ppb (19 October), ∼3–6 ppb (20 October), and ∼5–10 ppb (21 October) during a typical haze-aggravating process vertically.

4. Surface O_3 was controlled by VOC-sensitive chemistry, while O_3 at higher altitude (>800 m) was controlled by NO_x-sensitive chemistry in NCP during autumn. The nitrate photolysis reaction enhanced OH and NO_x concentrations, and both favored O_3 formation at high altitude, especially in haze-aggravating processes with abundant nitrate. The produced HONO rather than the produced NO_2 through nitrate photolysis had a stronger promotion of O_3 formation near the surface, but the impacts of the two products on O_3 enhancements were similar at higher altitude (∼2000 m).

5. Nitrate photolysis only contributed ∼5 % of the surface HONO in the daytime with a $J_{nitrate}/J_{HNO_3}$ ratio of 30 ($\sim 1 \times 10^{-5}$ s^{-1}) but contributed ∼30 %–50 % of the enhanced O_3 near the surface in NCP on hazy days. The photolysis of nitrate had a limited impact on nitrate concentrations (reduced by <5 % with $J_{nitrate}/J_{HNO_3} = 30$, and <15 % even with a $J_{nitrate}/J_{HNO_3}$ ratio of 120), due mainly to the simultaneously enhanced atmospheric oxidants favoring the formation of HNO_3 and nitrate. Choosing a larger $J_{nitrate}$ value might cover up other ground-based unknown HONO sources, but overestimate vertical sources of HONO as well as NO_x and O_3 concentrations; thus, more studies are needed to find the exact value of $J_{nitrate}$ in the real atmosphere.

Code and data availability. Data are available upon reasonable request to the corresponding authors. The code of the WRF-Chem model can be achieved from https://www2.acom.ucar.edu/wrf-chem (last access: 4 March 2022, NCAR/UCAR, 2022).

Supplement. The supplement related to this article is available online at: https://doi.org/10.5194/acp-22-3275-2022-supplement.

Author contributions. JZ, CL, JA, MG, and WW conceived and designed the research. JZ performed WRF-Chem simulations and wrote the paper. JZ, CL, YG, and HR performed data analyses and produced the figures. CL, YZ, FZ, XF, CY, KRD, YL, and MK conducted the field observations. WW, JA, MG, YL, and MK reviewed the article.

Competing interests. The contact author has declared that neither they nor their co-authors have any competing interests.

Disclaimer. Publisher's note: Copernicus Publications remains neutral with regard to jurisdictional claims in published maps and institutional affiliations.

Acknowledgements. This research was partially supported by the National Natural Science Foundation of China (Grant No. 92044302, 42075108, 42107124, 42075110, 41822703, 91544221, 91844301), Beijing National Laboratory for Molecular Sciences (BNLMS-CXXM-202011) and the China Postdoctoral Science Foundation (grant no. 2019M660764).

Financial support. This research has been supported by the National Natural Science Foundation of China (grant nos. 92044302, 42075108, 42107124, 42075110, 41822703, 91544221, and 91844301), the Beijing National Laboratory for Molecular Sciences (grant no. BNLMS-CXXM-202011), and the China Postdoctoral Science Foundation (grant no. 2019M660764).

Review statement. This paper was edited by Ivan Kourtchev and reviewed by three anonymous referees.

References

Alicke, B., Platt, U., and Stutz, J.: Impact of nitrous acid photolysis on the total hydroxyl radical budget during the Limitation of Oxidant Production/Pianura Padana Produzione di Ozono study in Milan, J. Geophys. Res.-Atmos., 107, 8196, https://doi.org/10.1029/2000jd000075, 2002.

An, J. L., Li, Y., Chen, Y., Li, J., Qu, Y., and Tang, Y. J.: Enhancements of major aerosol components due to additional HONO sources in the North China Plain and implications for visibility and haze, Adv. Atmos. Sci., 30, 57–66, https://doi.org/10.1007/s00376-012-2016-9, 2013.

Aumont, B., Chervier, F., and Laval, S.: Contribution of HONO sources to the $NO_x/HO_x/O_3$ chemistry in the polluted boundary layer, Atmos. Environ., 37, 487–498, https://doi.org/10.1016/S1352-2310(02)00920-2, 2003.

Avnery, S., Mauzerall, D. L., Liu, J., and Horowitz, L. W.: Global crop yield reductions due to surface ozone exposure: 1. Year 2000 crop production losses and economic damage, Atmos. Environ., 45, 2284–2296, https://doi.org/10.1016/j.atmosenv.2011.01.002, 2011a.

Avnery, S., Mauzerall, D. L., Liu, J., and Horowitz, L. W.: Global crop yield reductions due to surface ozone exposure: 2. Year 2030 potential crop production losses and economic damage under two scenarios of O_3 pollution, Atmos. Environ., 45, 2297–2309, https://doi.org/10.1016/j.atmosenv.2010.11.045, 2011b.

Baergen, A. M. and Donaldson, D. J.: Photochemical renoxification of nitric acid on real urban grime, Environ. Sci. Technol., 47, 815–820, https://doi.org/10.1021/es3037862, 2013.

Bao, F., Li, M., Zhang, Y., Chen, C., and Zhao, J.: Photochemical Aging of Beijing Urban $PM_{2.5}$: HONO Production, Environ. Sci. Technol., 52, 6309–6316, https://doi.org/10.1021/acs.est.8b00538, 2018.

Bao, F. X., Jiang, H. Y., Zhang, Y., Li, M., Ye, C. X., Wang, W. G., Ge, M. F., Chen, C. C., and Zhao, J. C.: The Key Role of Sulfate in the Photochemical Renoxification on Real $PM_{2.5}$, Environ. Sci. Technol., 54, 3121–3128, https://doi.org/10.1021/acs.est.9b06764, 2020.

Bejan, I., Abd-el-Aal, Y., Barnes, I., Benter, T., Bohn, B., Wiesen, P., and Kleffmann, J.: The photolysis of ortho-nitrophenols: a new gas phase source of HONO, Phys. Chem. Chem. Phys., 8, 2028–2035, https://doi.org/10.1039/b516590c, 2006.

Chen, S., Wang, H., Lu, K., Zeng, L., Hu, M., and Zhang, Y.: The trend of surface ozone in Beijing from 2013 to 2019: Indications of the persisting strong atmospheric oxidation capacity, Atmos. Environ., 242, 117801, https://doi.org/10.1016/j.atmosenv.2020.117801, 2020.

Chen, Y., Wang, W. G., Lian, C. F., Peng, C., Zhang, W. Y., Li, J. L., Liu, M. Y., Shi, B., Wang, X. F., and Ge, M. F.: Evaluation and impact factors of indoor and outdoor gas-phase nitrous acid under different environmental conditions, J. Environ. Sci., 95, 165–171, https://doi.org/10.1016/j.jes.2020.03.048, 2020.

Chen, Y., Zheng, P., Wang, Z., Pu, W., Tan, Y., Yu, C., Xia, M., Wang, W., Guo, J., Huang, D., Yan, C., Nie, W., Ling, Z., Chen, Q., Lee, S., and Wang, T.: Secondary formation and impacts of gaseous nitro-phenolic compounds in the continental outflow observed at a background site in south China, Environ. Sci. Technol., https://doi.org/10.1021/acs.est.1c04596, 2021.

Crowley, J. N. and Carl, S. A.: OH formation in the photoexcitation of NO_2 beyond the dissociation threshold in the presence of water vapor, J. Phys. Chem. A, 101, 4178–4184, https://doi.org/10.1021/jp970319e, 1997.

Cui, L., Li, R., Fu, H., Meng, Y., Zhao, Y., Li, Q., and Chen, J.: Nitrous acid emission from open burning of major crop residues in mainland China, Atmos. Environ., 244, 117950, https://doi.org/10.1016/j.atmosenv.2020.117950, 2021.

Dillon, T. J. and Crowley, J. N.: Reactive quenching of electronically excited NO_2^* and NO_3^* by H_2O as potential sources of atmospheric HO_x radicals, Atmos. Chem. Phys., 18, 14005–14015, https://doi.org/10.5194/acp-18-14005-2018, 2018.

Dong, W., Xing, J., and Wang, S.: Temporal and spatial distribution of anthropogenic ammonia emissions in China: 1994–2006, Environmental Sciences, 31, 1457–1463, 2010 (in Chinese).

Emmons, L. K., Walters, S., Hess, P. G., Lamarque, J.-F., Pfister, G. G., Fillmore, D., Granier, C., Guenther, A., Kinnison, D., Laepple, T., Orlando, J., Tie, X., Tyndall, G., Wiedinmyer, C., Baughcum, S. L., and Kloster, S.: Description and evaluation of the Model for Ozone and Related chemical Tracers, version 4 (MOZART-4), Geosci. Model Dev., 3, 43–67, https://doi.org/10.5194/gmd-3-43-2010, 2010.

Feng, T., Zhao, S., Bei, N., Liu, S., and Li, G.: Increasing atmospheric oxidizing capacity weakens emission mitigation effort in Beijing during autumn haze events, Chemosphere, 281, 130855, https://doi.org/10.1016/j.chemosphere.2021.130855, 2021.

Feng, Z., Hu, E., Wang, X., Jiang, L., and Liu, X.: Ground-level O_3 pollution and its impacts on food crops in China: a review, Environ. Pollut., 199, 42–48, https://doi.org/10.1016/j.envpol.2015.01.016, 2015.

Feng, Z., De Marco, A., Anav, A., Gualtieri, M., Sicard, P., Tian, H., Fornasier, F., Tao, F., Guo, A., and Paoletti, E.: Economic losses due to ozone impacts on human health, forest productivity and crop yield across China, Environ. Int., 131, 104966, https://doi.org/10.1016/j.envint.2019.104966, 2019.

Feng, Z., Xu, Y., Kobayashi, K., Dai, L., Zhang, T., Agathokleous, E., Calatayud, V., Paoletti, E., Mukherjee, A., Agrawal, M., Park, R. J., Oak, Y. J., and Yue, X.: Ozone pollution threatens the production of major staple crops in East Asia, Nat. Food, 3, 47–56, https://doi.org/10.1038/s43016-021-00422-6, 2022.

Finlayson-Pitts, B. J., Wingen, L. M., Sumner, A. L., Syomin, D., and Ramazan, K. A.: The heterogeneous hydrolysis of NO_2 in laboratory systems and in outdoor and indoor atmospheres: An integrated mechanism, Phys. Chem. Chem. Phys., 5, 223–242, https://doi.org/10.1039/b208564j, 2003.

Fröhlich, R., Cubison, M. J., Slowik, J. G., Bukowiecki, N., Prévôt, A. S. H., Baltensperger, U., Schneider, J., Kimmel, J. R., Gonin, M., Rohner, U., Worsnop, D. R., and Jayne, J. T.: The ToF-ACSM: a portable aerosol chemical speciation monitor with TOFMS detection, Atmos. Meas. Tech., 6, 3225–3241, https://doi.org/10.5194/amt-6-3225-2013, 2013.

Fu, X., Wang, T., Zhang, L., Li, Q., Wang, Z., Xia, M., Yun, H., Wang, W., Yu, C., Yue, D., Zhou, Y., Zheng, J., and Han, R.: The significant contribution of HONO to secondary pollutants during a severe winter pollution event in southern China, Atmos. Chem. Phys., 19, 1–14, https://doi.org/10.5194/acp-19-1-2019, 2019.

Fu, X., Wang, T., Gao, J., Wang, P., Liu, Y.M., Wang, S. X., Zhao, B., and Xue, L. K.: Persistent Heavy Winter Nitrate Pollution Driven by Increased Photochemical Oxidants in Northern China, Environ. Sci. Technol., 54, 3881–3889, https://doi.org/10.1021/acs.est.9b07248, 2020.

Gao, W., Tan, G., Hong, Y., Li, M., Nian, H., Guo, C., Huang, Z., Fu, Z., Dong, J., and Xu, X.: Development of portable single photon ionization time-of-flight mass spectrometer combined with membrane inlet, Int. J. Mass Spectrom., 334, 8–12, https://doi.org/10.1016/j.ijms.2012.09.003, 2013.

Ge, M., Tong, S., Wang, W., Zhang, W., Chen, M., Peng, C., Li, J., Zhou, L., Chen, Y., and Liu, M.: Important Oxidants and Their Impact on the Environmental Effects of Aerosols, J. Phys. Chem. A, 125, 3813–3825, https://doi.org/10.1021/acs.jpca.0c10236, 2021.

Ge, S., Wang, G., Zhang, S., Li, D., Xie, Y., Wu, C., Yuan, Q., Chen, J., and Zhang, H.: Abundant NH_3 in China Enhances Atmospheric HONO Production by Promoting the Heterogeneous Reaction of SO_2 with NO_2, Environ. Sci. Technol., 53, 14339–14347, https://doi.org/10.1021/acs.est.9b04196, 2019.

Gen, M., Liang, Z., Zhang, R., Go Mabato, B. R., and Chan, C. K.: Particulate nitrate photolysis in the atmosphere, Environ. Sci. Atmos., https://doi.org/10.1039/d1ea00087j, 2022.

Gligorovski, S., Strekowski, R., Barbati, S., and Vione, D.: Environmental Implications of Hydroxyl Radicals ($^{\bullet}OH$), Chem. Rev., 115, 13051–13092, https://doi.org/10.1021/cr500310b, 2015.

Gómez Alvarez, E., Sörgel, M., Gligorovski, S., Bassil, S., Bartolomei, V., Coulomb, B., Zetzsch, C., and Wortham, H.: Light-induced nitrous acid (HONO) production from NO_2 heteroge-

neous reactions on household chemicals, Atmos. Environ., 95, 391–399, https://doi.org/10.1016/j.atmosenv.2014.06.034, 2014.

Grell, G. A., Peckham, S. E., Schmitz, R., McKeen, S. A., Frost, G., Skamarock, W. C., and Eder, B.: Fully coupled "online" chemistry within the WRF model, Atmos. Environ., 39, 6957–6975, https://doi.org/10.1016/j.atmosenv.2005.04.027, 2005.

Guenther, A. B., Jiang, X., Heald, C. L., Sakulyanontvittaya, T., Duhl, T., Emmons, L. K., and Wang, X.: The Model of Emissions of Gases and Aerosols from Nature version 2.1 (MEGAN2.1): an extended and updated framework for modeling biogenic emissions, Geosci. Model Dev., 5, 1471–1492, https://doi.org/10.5194/gmd-5-1471-2012, 2012.

Guo, Y., Zhang, J., An, J., Qu, Y., Liu, X., Sun, Y., and Chen, Y.: Effect of vertical parameterization of a missing daytime source of HONO on concentrations of HONO, O_3 and secondary organic aerosols in eastern China, Atmos. Environ., 226, 117208, https://doi.org/10.1016/j.atmosenv.2019.117208, 2020.

Hendrick, F., Müller, J.-F., Clémer, K., Wang, P., De Mazière, M., Fayt, C., Gielen, C., Hermans, C., Ma, J. Z., Pinardi, G., Stavrakou, T., Vlemmix, T., and Van Roozendael, M.: Four years of ground-based MAX-DOAS observations of HONO and NO_2 in the Beijing area, Atmos. Chem. Phys., 14, 765–781, https://doi.org/10.5194/acp-14-765-2014, 2014.

Huang, X., Li, M. M., Li, J. F., and Song, Y.: A high-resolution emission inventory of crop burning in fields in China based on MODIS Thermal Anomalies/Fire products, Atmos. Environ., 50, 9–15, https://doi.org/10.1016/j.atmosenv.2012.01.017, 2012.

Kasibhatla, P., Sherwen, T., Evans, M. J., Carpenter, L. J., Reed, C., Alexander, B., Chen, Q., Sulprizio, M. P., Lee, J. D., Read, K. A., Bloss, W., Crilley, L. R., Keene, W. C., Pszenny, A. A. P., and Hodzic, A.: Global impact of nitrate photolysis in sea-salt aerosol on NO_x, OH, and O_3 in the marine boundary layer, Atmos. Chem. Phys., 18, 11185–11203, https://doi.org/10.5194/acp-18-11185-2018, 2018.

Kim, S., VandenBoer, T. C., Young, C. J., Riedel, T. P., Thornton, J. A., Swarthout, B., Sive, B., Lerner, B., Gilman, J. B., Warneke, C., Roberts, J. M., Guenther, A., Wagner, N. L., Dube, W. P., Williams, E., and Brown, S. S.: The primary and recycling sources of OH during the NACHTT-2011 campaign: HONO as an important OH primary source in the wintertime, J. Geophys. Res.-Atmos., 119, 6886–6896, https://doi.org/10.1002/2013jd019784, 2014.

Kleffmann, J., Kurtenbach, R., Lorzer, J., Wiesen, P., Kalthoff, N., Vogel, B., and Vogel, H.: Measured and simulated vertical profiles of nitrous acid – Part I: Field measurements, Atmos. Environ., 37, 2949–2955, https://doi.org/10.1016/S1352-2310(03)00242-5, 2003.

Klosterkother, A., Kurtenbach, R., Wiesen, P., and Kleffmann, J.: Determination of the emission indices for NO, NO_2, HONO, HCHO, CO, and particles emitted from candles, Indoor Air, 31, 116–127, https://doi.org/10.1111/ina.12714, 2021.

Kramer, L. J., Crilley, L. R., Adams, T. J., Ball, S. M., Pope, F. D., and Bloss, W. J.: Nitrous acid (HONO) emissions under real-world driving conditions from vehicles in a UK road tunnel, Atmos. Chem. Phys., 20, 5231–5248, https://doi.org/10.5194/acp-20-5231-2020, 2020.

Kubota, M. and Asami, T.: Volatilization of Nitrous-Acid from Upland Soils, J. Soil Sci. Plant Nutr., 31, 27–34, https://doi.org/10.1080/17470765.1985.10555214, 1985.

Kurtenbach, R., Becker, K. H., Gomes, J. A. G., Kleffmann, J., Lorzer, J. C., Spittler, M., Wiesen, P., Ackermann, R., Geyer, A., and Platt, U.: Investigations of emissions and heterogeneous formation of HONO in a road traffic tunnel, Atmos. Environ., 35, 3385–3394, https://doi.org/10.1016/S1352-2310(01)00138-8, 2001.

Laufs, S. and Kleffmann, J.: Investigations on HONO formation from photolysis of adsorbed HNO_3 on quartz glass surfaces, Phys. Chem. Chem. Phys., 18, 9616–9625, https://doi.org/10.1039/c6cp00436a, 2016.

Lee, J. D., Whalley, L. K., Heard, D. E., Stone, D., Dunmore, R. E., Hamilton, J. F., Young, D. E., Allan, J. D., Laufs, S., and Kleffmann, J.: Detailed budget analysis of HONO in central London reveals a missing daytime source, Atmos. Chem. Phys., 16, 2747–2764, https://doi.org/10.5194/acp-16-2747-2016, 2016.

Li, G., Lei, W., Zavala, M., Volkamer, R., Dusanter, S., Stevens, P., and Molina, L. T.: Impacts of HONO sources on the photochemistry in Mexico City during the MCMA-2006/MILAGO Campaign, Atmos. Chem. Phys., 10, 6551–6567, https://doi.org/10.5194/acp-10-6551-2010, 2010.

Li, K., Jacob, D. J., Shen, L., Lu, X., De Smedt, I., and Liao, H.: Increases in surface ozone pollution in China from 2013 to 2019: anthropogenic and meteorological influences, Atmos. Chem. Phys., 20, 11423–11433, https://doi.org/10.5194/acp-20-11423-2020, 2020.

Li, L., Chen, C. H., Huang, C., Huang, H. Y., Zhang, G. F., Wang, Y. J., Wang, H. L., Lou, S. R., Qiao, L. P., Zhou, M., Chen, M. H., Chen, Y. R., Streets, D. G., Fu, J. S., and Jang, C. J.: Process analysis of regional ozone formation over the Yangtze River Delta, China using the Community Multi-scale Air Quality modeling system, Atmos. Chem. Phys., 12, 10971–10987, https://doi.org/10.5194/acp-12-10971-2012, 2012.

Li, M., Zhang, Q., Kurokawa, J.-I., Woo, J.-H., He, K., Lu, Z., Ohara, T., Song, Y., Streets, D. G., Carmichael, G. R., Cheng, Y., Hong, C., Huo, H., Jiang, X., Kang, S., Liu, F., Su, H., and Zheng, B.: MIX: a mosaic Asian anthropogenic emission inventory under the international collaboration framework of the MICS-Asia and HTAP, Atmos. Chem. Phys., 17, 935–963, https://doi.org/10.5194/acp-17-935-2017, 2017.

Li, S., Matthews, J., and Sinha, A.: Atmospheric hydroxyl radical production from electronically excited NO_2 and H_2O, Science, 319, 1657–1660, https://doi.org/10.1126/science.1151443, 2008.

Li, X., Rohrer, F., Hofzumahaus, A., Brauers, T., Haseler, R., Bohn, B., Broch, S., Fuchs, H., Gomm, S., Holland, F., Jager, J., Kaiser, J., Keutsch, F. N., Lohse, I., Lu, K., Tillmann, R., Wegener, R., Wolfe, G. M., Mentel, T. F., Kiendler-Scharr, A., and Wahner, A.: Missing gas-phase source of HONO inferred from Zeppelin measurements in the troposphere, Science, 344, 292–296, https://doi.org/10.1126/science.1248999, 2014.

Li, X., Rohrer, F., Hofzumahaus, A., Brauers, T., Häseler, R., Bohn, B., Broch, S., Fuchs, H., Gomm, S., and Holland, F.: Response to Comment on "Missing gas-phase source of HONO inferred from Zeppelin measurements in the troposphere", Science, 348, 1326–1326, https://doi.org/10.1126/science.aab1122, 2015.

Li, Y., An, J. L., Min, M., Zhang, W., Wang, F., and Xie, P. H.: Impacts of HONO sources on the air quality in Beijing, Tianjin and Hebei Province of China, Atmos. Environ., 45, 4735–4744, https://doi.org/10.1016/j.atmosenv.2011.04.086, 2011.

Liao, S., Zhang, J., Yu, F., Zhu, M., Liu, J., Ou, J., Dong, H., Sha, Q., Zhong, Z., Xie, Y., Luo, H., Zhang, L., and Zheng, J.: High Gaseous Nitrous Acid (HONO) Emissions from Light-Duty Diesel Vehicles, Environ. Sci. Technol., 55, 200–208, https://doi.org/10.1021/acs.est.0c05599, 2021.

Lin, Y. L., Farley, R. D., and Orville, H. D.: Bulk Parameterization of the Snow Field in a Cloud Model, J. Clim. Appl. Meteorol., 22, 1065–1092, https://doi.org/10.1175/1520-0450(1983)022<1065:Bpotsf>2.0.Co;2, 1983.

Liu, J., Li, S., Zeng, J., Mekic, M., Yu, Z., Zhou, W., Loisel, G., Gandolfo, A., Song, W., Wang, X., Zhou, Z., Herrmann, H., Li, X., and Gligorovski, S.: Assessing indoor gas phase oxidation capacity through real-time measurements of HONO and NO_x in Guangzhou, China, Environ. Sci.: Processes Impacts, 21, 1393–1402, https://doi.org/10.1039/c9em00194h, 2019.

Liu, Y., Zhang, Y., Lian, C., Yan, C., Feng, Z., Zheng, F., Fan, X., Chen, Y., Wang, W., Chu, B., Wang, Y., Cai, J., Du, W., Daellenbach, K. R., Kangasluoma, J., Bianchi, F., Kujansuu, J., Petäjä, T., Wang, X., Hu, B., Wang, Y., Ge, M., He, H., and Kulmala, M.: The promotion effect of nitrous acid on aerosol formation in wintertime in Beijing: the possible contribution of traffic-related emissions, Atmos. Chem. Phys., 20, 13023–13040, https://doi.org/10.5194/acp-20-13023-2020, 2020.

Liu, Z., Wang, Y., Costabile, F., Amoroso, A., Zhao, C., Huey, L. G., Stickel, R., Liao, J., and Zhu, T.: Evidence of aerosols as a media for rapid daytime HONO production over China, Environ. Sci. Technol., 48, 14386–14391, https://doi.org/10.1021/es504163z, 2014.

Lu, X., Zhang, L., Wang, X. L., Gao, M., Li, K., Zhang, Y. Z., Yue, X., and Zhang, Y. H.: Rapid Increases in Warm-Season Surface Ozone and Resulting Health Impact in China Since 2013, Environ. Sci. Technol. Lett., 7, 240–247, https://doi.org/10.1021/acs.estlett.0c00171, 2020.

Ma, J., Liu, Y., Han, C., Ma, Q., Liu, C., and He, H.: Review of heterogeneous photochemical reactions of NO_y on aerosol – A possible daytime source of nitrous acid (HONO) in the atmosphere, J. Environ. Sci., 25, 326–334, https://doi.org/10.1016/s1001-0742(12)60093-x, 2013.

Ma, Z., Xu, J., Quan, W., Zhang, Z., Lin, W., and Xu, X.: Significant increase of surface ozone at a rural site, north of eastern China, Atmos. Chem. Phys., 16, 3969–3977, https://doi.org/10.5194/acp-16-3969-2016, 2016.

Maji, K. J. and Namdeo, A.: Continuous increases of surface ozone and associated premature mortality growth in China during 2015–2019, Environ. Pollut., 269, 116183, https://doi.org/10.1016/j.envpol.2020.116183, 2021.

Marion, A., Morin, J., Gandolfo, A., Ormeno, E., D'Anna, B., and Wortham, H.: Nitrous acid formation on Zea mays leaves by heterogeneous reaction of nitrogen dioxide in the laboratory, Environ. Res., 193, 110543, https://doi.org/10.1016/j.envres.2020.110543, 2021.

Meng, F., Qin, M., Tang, K., Duan, J., Fang, W., Liang, S., Ye, K., Xie, P., Sun, Y., Xie, C., Ye, C., Fu, P., Liu, J., and Liu, W.: High-resolution vertical distribution and sources of HONO and NO_2 in the nocturnal boundary layer in urban Beijing, China, Atmos. Chem. Phys., 20, 5071–5092, https://doi.org/10.5194/acp-20-5071-2020, 2020.

Mills, G., Buse, A., Gimeno, B., Bermejo, V., Holland, M., Emberson, L., and Pleijel, H.: A synthesis of AOT40-based response functions and critical levels of ozone for agricultural and horticultural crops, Atmos. Environ., 41, 2630–2643, https://doi.org/10.1016/j.atmosenv.2006.11.016, 2007.

Mills, G., Sharps, K., Simpson, D., Pleijel, H., Broberg, M., Uddling, J., Jaramillo, F., Davies, W. J., Dentener, F., Van den Berg, M., Agrawal, M., Agrawal, S. B., Ainsworth, E. A., Buker, P., Emberson, L., Feng, Z., Harmens, H., Hayes, F., Kobayashi, K., Paoletti, E., and Van Dingenen, R.: Ozone pollution will compromise efforts to increase global wheat production, Glob. Change Biol., 24, 3560–3574, https://doi.org/10.1111/gcb.14157, 2018.

National Centers for Environmental Prediction, National Weather Service, NOAA, and U.S. Department of Commerce: NCEP FNL Operational Model Global Tropospheric Analyses, Continuing From July 1999, Research Data Archive at the National Center for Atmospheric Research, Computational and Information Systems Laboratory, Boulder [data set], https://doi.org/10.5065/D6M043C6, 2000.

NCAR/UCAR: WRF-Chem, NCAR/UCAR [code], https://www2.acom.ucar.edu/wrf-chem, last access: 4 March 2022.

Oswald, R., Behrendt, T., Ermel, M., Wu, D., Su, H., Cheng, Y., Breuninger, C., Moravek, A., Mougin, E., Delon, C., Loubet, B., Pommerening-Roser, A., Sörgel, M., Pöschl, U., Hoffmann, T., Andreae, M. O., Meixner, F. X., and Trebs, I.: HONO emissions from soil bacteria as a major source of atmospheric reactive nitrogen, Science, 341, 1233–1235, https://doi.org/10.1126/science.1242266, 2013.

Pagsberg, P., Bjergbakke, E., Ratajczak, E., and Sillesen, A.: Kinetics of the gas phase reaction $OH + NO\ (+M) \rightarrow HONO\ (+M)$ and the determination of the UV absorption cross sections of HONO, Chem. Phys. Lett., 272, 383–390, https://doi.org/10.1016/S0009-2614(97)00576-9, 1997.

Perner, D. and Platt, U.: Detection of nitrous acid in the atmospeere by differential optical absorption, Geophys. Res. Lett., 6, 917–920, https://doi.org/10.1029/GL006i012p00917, 1979.

Pitts, J. N., Wallington, T. J., Biermann, H. W., and Winer, A. M.: Identification and Measurement of Nitrous-Acid in an Indoor Environment, Atmos. Environ., 19, 763–767, https://doi.org/10.1016/0004-6981(85)90064-2, 1985.

Qu, Y., Chen, Y., Liu, X., Zhang, J., Guo, Y., and An, J.: Seasonal effects of additional HONO sources and the heterogeneous reactions of N_2O_5 on nitrate in the North China Plain, Sci. Total Environ., 690, 97–107, https://doi.org/10.1016/j.scitotenv.2019.06.436, 2019.

Reed, C., Evans, M. J., Crilley, L. R., Bloss, W. J., Sherwen, T., Read, K. A., Lee, J. D., and Carpenter, L. J.: Evidence for renoxification in the tropical marine boundary layer, Atmos. Chem. Phys., 17, 4081–4092, https://doi.org/10.5194/acp-17-4081-2017, 2017.

Richards, B. L., Middleton, J. T., and Hewitt, W. B.: Air Pollution With Relation to Agronomic Crops: V. Oxidant Stipple of Grape, Agron. J., 50, 559–561, 1958.

Rohrer, F., Bohn, B., Brauers, T., Brüning, D., Johnen, F.-J., Wahner, A., and Kleffmann, J.: Characterisation of the photolytic HONO-source in the atmosphere simulation chamber SAPHIR, Atmos. Chem. Phys., 5, 2189–2201, https://doi.org/10.5194/acp-5-2189-2005, 2005.

Romer, P. S., Wooldridge, P. J., Crounse, J. D., Kim, M. J., Wennberg, P. O., Dibb, J. E., Scheuer, E., Blake, D. R., Meinardi, S., Brosius, A. L., Thames, A. B., Miller, D. O., Brune, W.

H., Hall, S. R., Ryerson, T. B., and Cohen, R. C.: Constraints on Aerosol Nitrate Photolysis as a Potential Source of HONO and NO_x, Environ. Sci. Technol., 52, 13738–13746, https://doi.org/10.1021/acs.est.8b03861, 2018.

Rondon, A. and Sanhueza, E.: High HONO atmospheric concentrations during vegetation burning in the tropical savannah, Tellus B, 41, 474–477, https://doi.org/10.1111/j.1600-0889.1989.tb00323.x, 1989.

Ryan, R. G., Rhodes, S., Tully, M., Wilson, S., Jones, N., Frieß, U., and Schofield, R.: Daytime HONO, NO_2 and aerosol distributions from MAX-DOAS observations in Melbourne, Atmos. Chem. Phys., 18, 13969–13985, https://doi.org/10.5194/acp-18-13969-2018, 2018.

Sakamaki, F., Hatakeyama, S., and Akimoto, H.: Formation of Nitrous-Acid and Nitric-Oxide in the Heterogeneous Dark Reaction of Nitrogen-Dioxide and Water-Vapor in a Smog Chamber, Int. J. Chem. Kinet., 15, 1013–1029, https://doi.org/10.1002/kin.550151006, 1983.

Saliba, N. A., Mochida, M., and Finlayson-Pitts, B. J.: Laboratory studies of sources of HONO in polluted urban atmospheres, Geophys. Res. Lett., 27, 3229–3232, https://doi.org/10.1029/2000gl011724, 2000.

Sarwar, G., Roselle, S. J., Mathur, R., Appel, W., Dennis, R. L., and Vogel, B.: A comparison of CMAQ HONO predictions with observations from the northeast oxidant and particle study, Atmos. Environ., 42, 5760–5770, https://doi.org/10.1016/j.atmosenv.2007.12.065, 2008.

Selin, N. E., Wu, S., Nam, K. M., Reilly, J. M., Paltsev, S., Prinn, R. G., and Webster, M. D.: Global health and economic impacts of future ozone pollution, Environ. Res. Lett., 4, 044014, https://doi.org/10.1088/1748-9326/4/4/044014, 2009.

Shi, Q., Tao, Y., Krechmer, J. E., Heald, C. L., Murphy, J. G., Kroll, J. H., and Ye, Q.: Laboratory Investigation of Renoxification from the Photolysis of Inorganic Particulate Nitrate, Environ. Sci. Technol., 55, 854–861, https://doi.org/10.1021/acs.est.0c06049, 2021.

Shi, X., Ge, Y., Zheng, J., Ma, Y., Ren, X., and Zhang, Y.: Budget of nitrous acid and its impacts on atmospheric oxidative capacity at an urban site in the central Yangtze River Delta region of China, Atmos. Environ., 238, 117725, https://doi.org/10.1016/j.atmosenv.2020.117725, 2020.

Sillman, S.: The use of NO_y, H_2O_2, and HNO_3 as indicators for ozone-NO_x-hydrocarbon sensitivity in urban locations, J. Geophys. Res.-Atmos., 100, 14175–14188, https://doi.org/10.1029/94JD02953, 1995.

Slater, E. J., Whalley, L. K., Woodward-Massey, R., Ye, C., Lee, J. D., Squires, F., Hopkins, J. R., Dunmore, R. E., Shaw, M., Hamilton, J. F., Lewis, A. C., Crilley, L. R., Kramer, L., Bloss, W., Vu, T., Sun, Y., Xu, W., Yue, S., Ren, L., Acton, W. J. F., Hewitt, C. N., Wang, X., Fu, P., and Heard, D. E.: Elevated levels of OH observed in haze events during wintertime in central Beijing, Atmos. Chem. Phys., 20, 14847–14871, https://doi.org/10.5194/acp-20-14847-2020, 2020.

Sörgel, M., Trebs, I., Serafimovich, A., Moravek, A., Held, A., and Zetzsch, C.: Simultaneous HONO measurements in and above a forest canopy: influence of turbulent exchange on mixing ratio differences, Atmos. Chem. Phys., 11, 841–855, https://doi.org/10.5194/acp-11-841-2011, 2011.

Stuhl, F. and Niki, H.: Flash Photochemical Study of the Reaction OH + NO + M Using Resonance Fluorescent Detection of OH, J. Chem. Phys., 57, 3677–3679, https://doi.org/10.1063/1.1678826, 1972.

Tan, Z., Rohrer, F., Lu, K., Ma, X., Bohn, B., Broch, S., Dong, H., Fuchs, H., Gkatzelis, G. I., Hofzumahaus, A., Holland, F., Li, X., Liu, Y., Liu, Y., Novelli, A., Shao, M., Wang, H., Wu, Y., Zeng, L., Hu, M., Kiendler-Scharr, A., Wahner, A., and Zhang, Y.: Wintertime photochemistry in Beijing: observations of RO_x radical concentrations in the North China Plain during the BEST-ONE campaign, Atmos. Chem. Phys., 18, 12391–12411, https://doi.org/10.5194/acp-18-12391-2018, 2018.

Tang, M., Huang, X., Lu, K., Ge, M., Li, Y., Cheng, P., Zhu, T., Ding, A., Zhang, Y., Gligorovski, S., Song, W., Ding, X., Bi, X., and Wang, X.: Heterogeneous reactions of mineral dust aerosol: implications for tropospheric oxidation capacity, Atmos. Chem. Phys., 17, 11727–11777, https://doi.org/10.5194/acp-17-11727-2017, 2017.

Tang, Y., An, J., Wang, F., Li, Y., Qu, Y., Chen, Y., and Lin, J.: Impacts of an unknown daytime HONO source on the mixing ratio and budget of HONO, and hydroxyl, hydroperoxyl, and organic peroxy radicals, in the coastal regions of China, Atmos. Chem. Phys., 15, 9381–9398, https://doi.org/10.5194/acp-15-9381-2015, 2015.

Theys, N., Volkamer, R., Mueller, J. F., Zarzana, K. J., Kille, N., Clarisse, L., De Smedt, I., Lerot, C., Finkenzeller, H., Hendrick, F., Koenig, T. K., Lee, C. F., Knote, C., Yu, H., and Van Roozendael, M.: Global nitrous acid emissions and levels of regional oxidants enhanced by wildfires, Nat. Geosci., 13, 681–686, https://doi.org/10.1038/s41561-020-0637-7, 2020.

Tie, X., Long, X., Li, G., Zhao, S., Cao, J., and Xu, J.: Ozone enhancement due to the photodissociation of nitrous acid in eastern China, Atmos. Chem. Phys., 19, 11267–11278, https://doi.org/10.5194/acp-19-11267-2019, 2019.

VandenBoer, T. C., Brown, S. S., Murphy, J. G., Keene, W. C., Young, C. J., Pszenny, A. A. P., Kim, S., Warneke, C., de Gouw, J. A., Maben, J. R., Wagner, N. L., Riedel, T. P., Thornton, J. A., Wolfe, D. E., Dube, W. P., Ozturk, F., Brock, C. A., Grossberg, N., Lefer, B., Lerner, B., Middlebrook, A. M., and Roberts, J. M.: Understanding the role of the ground surface in HONO vertical structure: High resolution vertical profiles during NACHTT-11, J. Geophys. Res.-Atmos., 118, 10155–10171, https://doi.org/10.1002/jgrd.50721, 2013.

Villena, G., Kleffmann, J., Kurtenbach, R., Wiesen, P., Lissi, E., Rubio, M.A., Croxatto, G., and Rappenglück, B.: Vertical gradients of HONO, NO_x and O_3 in Santiago de Chile, Atmos. Environ., 45, 3867–3873, https://doi.org/10.1016/j.atmosenv.2011.01.073, 2011.

Wang, F., An, J. L., Li, Y., Tang, Y. J., Lin, J., Qu, Y., Chen, Y., Zhang, B., and Zhai, J.: Impacts of uncertainty in AVOC emissions on the summer RO_x budget and ozone production rate in the three most rapidly-developing economic growth regions of China, Adv. Atmos. Sci., 31, 1331–1342, https://doi.org/10.1007/s00376-014-3251-z, 2014.

Wang, X., Zhang, Y., Hu, Y., Zhou, W., Lu, K., Zhong, L., Zeng, L., Shao, M., Hu, M., and Russell, A. G.: Process analysis and sensitivity study of regional ozone formation over the Pearl River Delta, China, during the PRIDE-PRD2004 campaign using the Community Multiscale Air Quality modeling system, At-

mos. Chem. Phys., 10, 4423–4437, https://doi.org/10.5194/acp-10-4423-2010, 2010.

Wang, Y., Dörner, S., Donner, S., Böhnke, S., De Smedt, I., Dickerson, R. R., Dong, Z., He, H., Li, Z., Li, Z., Li, D., Liu, D., Ren, X., Theys, N., Wang, Y., Wang, Y., Wang, Z., Xu, H., Xu, J., and Wagner, T.: Vertical profiles of NO_2, SO_2, HONO, HCHO, CHOCHO and aerosols derived from MAX-DOAS measurements at a rural site in the central western North China Plain and their relation to emission sources and effects of regional transport, Atmos. Chem. Phys., 19, 5417–5449, https://doi.org/10.5194/acp-19-5417-2019, 2019.

Wang, Y., Apituley, A., Bais, A., Beirle, S., Benavent, N., Borovski, A., Bruchkouski, I., Chan, K. L., Donner, S., Drosoglou, T., Finkenzeller, H., Friedrich, M. M., Frieß, U., Garcia-Nieto, D., Gómez-Martín, L., Hendrick, F., Hilboll, A., Jin, J., Johnston, P., Koenig, T. K., Kreher, K., Kumar, V., Kyuberis, A., Lampel, J., Liu, C., Liu, H., Ma, J., Polyansky, O. L., Postylyakov, O., Querel, R., Saiz-Lopez, A., Schmitt, S., Tian, X., Tirpitz, J.-L., Van Roozendael, M., Volkamer, R., Wang, Z., Xie, P., Xing, C., Xu, J., Yela, M., Zhang, C., and Wagner, T.: Inter-comparison of MAX-DOAS measurements of tropospheric HONO slant column densities and vertical profiles during the CINDI-2 campaign, Atmos. Meas. Tech., 13, 5087–5116, https://doi.org/10.5194/amt-13-5087-2020, 2020.

Wilkinson, S., Mills, G., Illidge, R., and Davies, W. J.: How is ozone pollution reducing our food supply?, J. Exp. Bot., 63, 527–536, https://doi.org/10.1093/jxb/err317, 2012.

Wong, K. W., Oh, H.-J., Lefer, B. L., Rappenglück, B., and Stutz, J.: Vertical profiles of nitrous acid in the nocturnal urban atmosphere of Houston, TX, Atmos. Chem. Phys., 11, 3595–3609, https://doi.org/10.5194/acp-11-3595-2011, 2011.

Wong, K. W., Tsai, C., Lefer, B., Haman, C., Grossberg, N., Brune, W. H., Ren, X., Luke, W., and Stutz, J.: Daytime HONO vertical gradients during SHARP 2009 in Houston, TX, Atmos. Chem. Phys., 12, 635–652, https://doi.org/10.5194/acp-12-635-2012, 2012.

Wu, D., Horn, M. A., Behrendt, T., Muller, S., Li, J., Cole, J. A., Xie, B., Ju, X., Li, G., Ermel, M., Oswald, R., Fröhlich-Nowoisky, J., Hoor, P., Hu, C., Liu, M., Andreae, M. O., Pöschl, U., Cheng, Y., Su, H., Trebs, I., Weber, B., and Sorgel, M.: Soil HONO emissions at high moisture content are driven by microbial nitrate reduction to nitrite: tackling the HONO puzzle, ISME J., 13, 1688–1699, https://doi.org/10.1038/s41396-019-0379-y, 2019.

Xing, C., Liu, C., Hu, Q., Fu, Q., Wang, S., Lin, H., Zhu, Y., Wang, S., Wang, W., and Javed, Z.: Vertical distributions of wintertime atmospheric nitrogenous compounds and the corresponding OH radicals production in Leshan, southwest China, J. Environ. Sci., 105, 44–55, https://doi.org/10.1016/j.jes.2020.11.019, 2021.

Xing, L., Wu, J., Elser, M., Tong, S., Liu, S., Li, X., Liu, L., Cao, J., Zhou, J., El-Haddad, I., Huang, R., Ge, M., Tie, X., Prévôt, A. S. H., and Li, G.: Wintertime secondary organic aerosol formation in Beijing–Tianjin–Hebei (BTH): contributions of HONO sources and heterogeneous reactions, Atmos. Chem. Phys., 19, 2343–2359, https://doi.org/10.5194/acp-19-2343-2019, 2019.

Xu, J., Zhang, Y. H., and Wang, W.: Numerical study on the impacts of heterogeneous reactions on ozone formation in the Beijing urban area, Adv. Atmos. Sci., 23, 605–614, https://doi.org/10.1007/s00376-006-0605-1, 2006.

Xu, W., Yang, W., Han, C., Yang, H., and Xue, X.: Significant influences of TiO_2 crystal structures on NO_2 and HONO emissions from the nitrates photolysis, J. Environ. Sci., 102, 198–206, https://doi.org/10.1016/j.jes.2020.09.016, 2021.

Xue, C., Zhang, C., Ye, C., Liu, P., Catoire, V., Krysztofiak, G., Chen, H., Ren, Y., Zhao, X., Wang, J., Zhang, F., Zhang, C., Zhang, J., An, J., Wang, T., Chen, J., Kleffmann, J., Mellouki, A., and Mu, Y.: HONO Budget and Its Role in Nitrate Formation in the Rural North China Plain, Environ. Sci. Technol., 54, 11048–11057, https://doi.org/10.1021/acs.est.0c01832, 2020.

Xue, C. Y., Ye, C., Zhang, C. L., Catoire, V., Liu, P. F., Gu, R. R., Zhang, J. W., Ma, Z. B., Zhao, X. X., Zhang, W. Q., Ren, Y. G., Krysztofiak, G., Tong, S. R., Xue, L. K., An, J. L., Ge, M. F., Mellouki, A., and Mu, Y. J.: Evidence for Strong HONO Emission from Fertilized Agricultural Fields and its Remarkable Impact on Regional O_3 Pollution in the Summer North China Plain, ACS Earth Space Chem., 5, 340–347, https://doi.org/10.1021/acsearthspacechem.0c00314, 2021.

Yang, K., Kong, L., Tong, S., Shen, J., Chen, L., Jin, S., Wang, C., Sha, F., and Wang, L.: Double High-Level Ozone and $PM_{2.5}$ Co-Pollution Episodes in Shanghai, China: Pollution Characteristics and Significant Role of Daytime HONO, Atmosphere, 12, 557, https://doi.org/10.3390/atmos12050557, 2021.

Yang, W., Han, C., Yang, H., and Xue, X.: Significant HONO formation by the photolysis of nitrates in the presence of humic acids, Environ. Pollut., 243, 679–686, https://doi.org/10.1016/j.envpol.2018.09.039, 2018.

Yang, W., Han, C., Zhang, T., Tang, N., Yang, H., and Xue, X.: Heterogeneous photochemical uptake of NO_2 on the soil surface as an important ground-level HONO source, Environ. Pollut., 271, 116289, https://doi.org/10.1016/j.envpol.2020.116289, 2021.

Ye, C., Zhou, X., Pu, D., Stutz, J., Festa, J., Spolaor, M., Cantrell, C., Mauldin, R. L., Weinheimer, A., and Haggerty, J.: Comment on "Missing gas-phase source of HONO inferred from Zeppelin measurements in the troposphere", Science, 348, 1326, https://doi.org/10.1126/science.aaa1992, 2015.

Ye, C., Gao, H., Zhang, N., and Zhou, X.: Photolysis of Nitric Acid and Nitrate on Natural and Artificial Surfaces, Environ. Sci. Technol., 50, 3530–3536, https://doi.org/10.1021/acs.est.5b05032, 2016a.

Ye, C., Zhou, X., Pu, D., Stutz, J., Festa, J., Spolaor, M., Tsai, C., Cantrell, C., Mauldin, R. L., Campos, T., Weinheimer, A., Hornbrook, R. S., Apel, E. C., Guenther, A., Kaser, L., Yuan, B., Karl, T., Haggerty, J., Hall, S., Ullmann, K., Smith, J. N., Ortega, J., and Knote, C.: Rapid cycling of reactive nitrogen in the marine boundary layer, Nature, 532, 489–491, https://doi.org/10.1038/nature17195, 2016b.

Ye, C., Zhang, N., Gao, H., and Zhou, X.: Photolysis of Particulate Nitrate as a Source of HONO and NO_x, Environ. Sci. Technol., 51, 6849–6856, https://doi.org/10.1021/acs.est.7b00387, 2017.

Zaveri, R. A., Easter, R. C., Fast, J. D., and Peters, L. K.: Model for Simulating Aerosol Interactions and Chemistry (MOSAIC), J. Geophys. Res.-Atmos., 113, D13204, https://doi.org/10.1029/2007jd008782, 2008.

Zhang, B. Q. and Tao, F. M.: Direct homogeneous nucleation of NO_2, H_2O, and NH_3 for the production of ammonium nitrate particles and HONO gas, Chem. Phys. Lett., 489, 143–147, https://doi.org/10.1016/j.cplett.2010.02.059, 2010.

Zhang, H. L., Li, J. Y., Ying, Q., Yu, J. Z., Wu, D., Cheng, Y., He, K. B., and Jiang, J. K.: Source apportionment of $PM_{2.5}$ nitrate and sulfate in China using a source-oriented chemical transport model, Atmos. Environ., 62, 228–242, https://doi.org/10.1016/j.atmosenv.2012.08.014, 2012.

Zhang, J., An, J., Qu, Y., Liu, X., and Chen, Y.: Impacts of potential HONO sources on the concentrations of oxidants and secondary organic aerosols in the Beijing-Tianjin-Hebei region of China, Sci. Total Environ., 647, 836–852, https://doi.org/10.1016/j.scitotenv.2018.08.030, 2019a.

Zhang, J., Chen, J., Xue, C., Chen, H., Zhang, Q., Liu, X., Mu, Y., Guo, Y., Wang, D., Chen, Y., Li, J., Qu, Y., and An, J.: Impacts of six potential HONO sources on HO_x budgets and SOA formation during a wintertime heavy haze period in the North China Plain, Sci. Total Environ., 681, 110–123, https://doi.org/10.1016/j.scitotenv.2019.05.100, 2019b.

Zhang, J., Guo, Y., Qu, Y., Chen, Y., Yu, R., Xue, C., Yang, R., Zhang, Q., Liu, X., Mu, Y., Wang, J., Ye, C., Zhao, H., Sun, Q., Wang, Z., and An, J.: Effect of potential HONO sources on peroxyacetyl nitrate (PAN) formation in eastern China in winter, J. Environ. Sci., 94, 81–87, https://doi.org/10.1016/j.jes.2020.03.039, 2020.

Zhang, J., Ran, H., Guo, Y., Xue, C., Liu, X., Qu, Y., Sun, Y., Zhang, Q., Mu, Y., Chen, Y., Wang, J., and An, J.: High crop yield losses induced by potential HONO sources – A modelling study in the North China Plain, Sci. Total Environ., 803, 149929, https://doi.org/10.1016/j.scitotenv.2021.149929, 2022.

Zhang, L., Wang, T., Zhang, Q., Zheng, J. Y., Xu, Z., and Lv, M. Y.: Potential sources of nitrous acid (HONO) and their impacts on ozone: A WRF-Chem study in a polluted subtropical region, J. Geophys. Res.-Atmos., 121, 3645–3662, https://doi.org/10.1002/2015jd024468, 2016.

Zhang, N., Zhou, X. L., Shepson, P. B., Gao, H. L., Alaghmand, M., and Stirm, B.: Aircraft measurement of HONO vertical profiles over a forested region, Geophys. Res. Lett., 36, L15820, https://doi.org/10.1029/2009gl038999, 2009.

Zhang, Q. and Geng, G.: Impact of clean air action on $PM_{2.5}$ pollution in China, Sci. China Earth Sci., 62, 1845–1846, https://doi.org/10.1007/s11430-019-9531-4, 2019.

Zhang, S., Sarwar, G., Xing, J., Chu, B., Xue, C., Sarav, A., Ding, D., Zheng, H., Mu, Y., Duan, F., Ma, T., and He, H.: Improving the representation of HONO chemistry in CMAQ and examining its impact on haze over China, Atmos. Chem. Phys., 21, 15809–15826, https://doi.org/10.5194/acp-21-15809-2021, 2021.

Zhang, W. Q., Tong, S. R., Jia, C. H., Wang, L. L., Liu, B. X., Tang, G. Q., Ji, D. S., Hu, B., Liu, Z. R., Li, W. R., Wang, Z., Liu, Y., Wang, Y. S., and Ge, M. F.: Different HONO Sources for Three Layers at the Urban Area of Beijing, Environ. Sci. Technol., 54, 12870–12880, https://doi.org/10.1021/acs.est.0c02146, 2020.

Zhao, H., Zhang, Y., Qi, Q., and Zhang, H.: Evaluating the Impacts of Ground-Level O_3 on Crops in China, Curr. Pollut. Rep., 7, 565–578, https://doi.org/10.1007/s40726-021-00201-8, 2021.

Zheng, H., Song, S., Sarwar, G., Gen, M., Wang, S., Ding, D., Chang, X., Zhang, S., Xing, J., Sun, Y., Ji, D., Chan, C.K., Gao, J., and McElroy, M. B.: Contribution of Particulate Nitrate Photolysis to Heterogeneous Sulfate Formation for Winter Haze in China, Environ. Sci. Technol. Lett., 7, 632–638, https://doi.org/10.1021/acs.estlett.0c00368, 2020.

Zhou, X., Gao, H., He, Y., Huang, G., Bertman, S. B., Civerolo, K., and Schwab, J.: Nitric acid photolysis on surfaces in low-NO_x environments: Significant atmospheric implications, Geophys. Res. Lett., 30, 2217, https://doi.org/10.1029/2003GL018620, 2003.

Zhu, C., Xiang, B., Zhu, L., and Cole, R.: Determination of absorption cross sections of surface-adsorbed HNO_3 in the 290–330 nm region by Brewster angle cavity ring-down spectroscopy, Chem. Phys. Lett., 458, 373–377, https://doi.org/10.1016/j.cplett.2008.04.125, 2008.

Zhu, Y. W., Liu, W. Q., Fang, J., Xie, P. H., Dou, K., Qin, M., and Si, F. Q.: Monitoring and Analysis of Vertical Profile of Atmospheric HONO, NO_2 in Boundary Layer of Beijing, Spectrosc. Spect. Anal., 31, 1078–1082, 2011 (in Chinese).